Human Molecular Genetics, 2011, Vol. 20, No. 4 ***731–751***
doi:10.1093/hmg/ddq519
Advance Access published on November 30, 2010

miRNA-132 orchestrates chromatin remodeling and translational control of the circadian clock

Matías Alvarez-Saavedra[1,†], Ghadi Antoun[1], Akiko Yanagiya[2], Reynaldo Oliva-Hernandez[1], Daniel Cornejo-Palma[1], Carolina Perez-Iratxeta[3], Nahum Sonenberg[2] and Hai-Ying M. Cheng[1,*]

[1]Ottawa Institute of Systems Biology and Department of Biochemistry, Microbiology and Immunology, University of Ottawa, 451 Smyth Road, Ottawa, Ont., Canada K1H 8M5, [2]Department of Biochemistry and McGill Cancer Center, McGill University, Montreal, Que., Canada H3G 1Y6, [3]Ottawa Hospital Research Institute (OHRI), 501 Smyth Road, Ottawa, Ont., Canada K1H 8L6

Received September 16, 2010; Revised and Accepted November 25, 2010

Mammalian circadian rhythms are synchronized to the external time by daily resetting of the suprachiasmatic nucleus (SCN) in response to light. As the master circadian pacemaker, the SCN coordinates the timing of diverse cellular oscillators in multiple tissues. Aberrant regulation of clock timing is linked to numerous human conditions, including cancer, cardiovascular disease, obesity, various neurological disorders and the hereditary disorder familial advanced sleep phase syndrome. Additionally, mechanisms that underlie clock resetting factor into the sleep and physiological disturbances experienced by night-shift workers and travelers with jet lag. The Ca^{2+}/cAMP response element-binding protein-regulated microRNA, miR-132, is induced by light within the SCN and attenuates its capacity to reset, or entrain, the clock. However, the specific targets that are regulated by miR-132 and underlie its effects on clock entrainment remained elusive until now. Here, we show that genes involved in chromatin remodeling (*Mecp2*, *Ep300*, *Jarid1a*) and translational control (*Btg2*, *Paip2a*) are direct targets of miR-132 in the mouse SCN. Coordinated regulation of these targets underlies miR-132-dependent modulation of *Period* gene expression and clock entrainment: the *mPer1* and *mPer2* promoters are bound to and transcriptionally activated by MeCP2, whereas PAIP2A and BTG2 suppress the translation of the PERIOD proteins by enhancing mRNA decay. We propose that miR-132 is selectively enriched for chromatin- and translation-associated target genes and is an orchestrator of chromatin remodeling and protein translation within the SCN clock, thereby fine-tuning clock entrainment. These findings will further our understanding of mechanisms governing clock entrainment and its involvement in human diseases.

INTRODUCTION

The daily oscillations in metabolism, physiology and behavior of nearly all living organisms are manifestations of an intrinsic timekeeping machinery (1). In mammals, the master circadian pacemaker resides in the suprachiasmatic nucleus (SCN) of the hypothalamus and synchronizes rhythms of peripheral oscillators. The circadian timing system plays a crucial role in adapting an organism to an ever-changing external environment imposed by the 24-h solar cycle, thus ensuring that all biological processes function at their optimum. As the gateway between the environment and the rest of the circadian timing system, the SCN has the unique ability to reset its clock phase in direct response to a light stimulus, which is relayed from the retina via the retinohypothalamic tract, by a process known as entrainment.

The molecular clockwork that underlies circadian rhythms resides within every cellular oscillator and is comprised of a series of interlocked positive and negative transcription/translation feedback loops that drive rhythmic expression of critical clock components. In mammals, heterodimers of the Per-ARNT-Sim domain helix–loop–helix proteins BMAL1 and CLOCK bind to E-box elements within the promoters of *Period* (*Per*) and *Cryptochrome* (*Cry*) genes and activate their transcription. Once the accumulation of PER and CRY proteins

*To whom correspondence should be addressed. Tel: +1 6135625800 ext. 8908; Fax: +1 6135625452; Email: mchen2@uottawa.ca
†Present address: Department of Neuronal Cell Biology, Center for Brain Research, Medical University of Vienna, Vienna A1090, Austria.

in the cytoplasm reaches a critical threshold, PER–CRY complexes translocate to the nucleus and feedback inhibit the transcription of their own genes by repressing CLOCK–BMAL1 activity. In addition to core clock timing mechanisms, transcriptional activation also underlies the entrainment process. Photic entrainment of the clock is accompanied by induced expression of the *Per* genes (as well as immediate early genes) in the SCN. Moreover, numerous studies have implicated the transcription factor Ca^{2+}/cAMP response element-binding protein (CREB) in light-induced gene transactivation and resetting of the circadian clock. Dysregulation of clock timing, arising from mutations in a number of core clock proteins and their regulators, has been linked to a host of human conditions, including cancer, obesity, cardiovascular disease, several neurological disorders and hereditary disorders such as familial advanced sleep phase syndrome and delayed sleep phase syndrome (2–4). Clearly, our understanding of the involvement of clock timing in human disease would be enhanced by novel insights into the molecular mechanisms that regulate circadian clock function.

The landscape of circadian clock regulation has become more complex in recent years with emerging evidence pointing to the involvement of other cellular mechanisms in addition to gene transcription via 'classical' transactivator proteins. The fact that ~10% of all mammalian transcripts are under circadian regulation (5) suggests that genome-wide mechanisms are in effect to actuate large-scale transcriptional regulation. Specifically, various epigenetic mechanisms that alter the architecture of chromatin, for example, DNA methylation and histone modification, have been implicated in clock timing processes. The rhythms of *Per* and *Cry* expression in the liver coincide with rhythmic histone H3 acetylation (generally considered a mark of active transcription) at their gene promoters (6). More recently, CLOCK has been demonstrated to possess histone acetyltransferase activity (7), whereas the histone deacetylase, SIRT1, regulates rhythmic H3 acetylation at the promoters of clock-controlled genes in the liver (8,9). Histone methylation has also been implicated in circadian clock regulation. The histone methyltransferase, EZH2, interacts with CLOCK–BMAL1 complexes and is recruited to the *mPer1* and *mPer2* promoters, where it catalyzes the methylation of histone H3 at lysine 27 (H3K27), generally considered a mark of transcriptional repression (10). Finally, the promoters of various clock genes, notably *Per1* and *Per2*, have been shown to undergo methylation in some human cancers, suggesting that DNA methylation may play a role in the deregulated expression of *Per* genes during carcinogenesis (11).

Besides the regulation of gene expression, recent studies highlight the importance of mechanisms which influence the steady-state levels of proteins in the control of the circadian clock. For instance, phosphorylation of PER1 and PER2 by casein kinase I epsilon results in targeting of the PER proteins for degradation by the ubiquitin-proteasome degradation pathway (12,13). FBXL3, an F-box protein, has been shown to target CRY1 and CRY2 for ubiquitination and protein degradation (14,15). On the other hand, mechanisms that regulate *de novo* protein synthesis are also likely to influence circadian clock processes. Expression of nocturnin, a deadenylase that controls mRNA decay (and consequently, protein translation) by shortening of the poly(A) tail, is rhythmic in multiple murine tissues and is induced by mitogenic signals (16). Most recently, a study revealed that light activates the mammalian target of rapamycin (mTOR) signaling pathway within the SCN (17). The downstream targets of the mTOR pathway, p70 S6 kinase (p70 S6K) and eukaryotic initiation factor 4E-binding protein 1 (4E-BP1), subsequently regulate the protein translation machinery.

microRNAs (miRNAs) have emerged as yet another avenue by which the circadian clock is regulated. By binding to partially complementary target sites within the 3′ untranslated regions (3′UTRs) of select messenger RNAs (mRNAs), miRNAs act as potent negative regulators of protein translation either by directing the mRNA for degradation or inhibiting its translation into the encoded protein (18). Each miRNA is capable of regulating multiple target genes, leading to complex changes in genetic networks by the action of a single miRNA. Despite the growing number of computational algorithms that predict possible targets for any given miRNA, relatively few bona fide miRNA targets have been identified and validated experimentally in specific cell or tissue types. Recently, our group discovered a miRNA, miR-132, that is induced robustly in the murine SCN in response to light stimulation (19). Light-inducible miR-132 expression in the SCN is dependent on the mitogen-activated protein kinase (MAPK)/extracellular signal-regulated kinase (ERK) signaling pathway as well as the CREB transcriptional pathway. *In vivo* knockdown of miR-132 expression in the SCN results in a potentiation of light-induced clock resetting, suggesting that endogenous miR-132 acts as a negative modulator of light responsiveness. However, the mechanism by which miR-132 influences light-induced clock resetting, or more specifically, the targets of miR-132 within the SCN that mediate its effect, remained unknown. Since the publication of our work on the role of miRNAs in the SCN clock, a number of studies have emerged that further support an involvement of miRNAs in clock timing processes (20–22).

To investigate the molecular mechanisms that underlie miR-132-dependent regulation of photic entrainment of the SCN clock, we generated transgenic mice that conditionally express miR-132 in the SCN and forebrain regions and used them, in combination with *in vivo* loss-of-function approaches, to functionally validate miR-132 targets. In this report, we show that miR-132 transgenic mice exhibit attenuation in light-induced resetting of behavioral rhythms, as well as a parallel reduction in PER1 and PER2 expression in the SCN following photic stimulation. Furthermore, we discovered that a subset of miR-132-regulated targets is implicated in chromatin remodeling (*Mecp2, Ep300, Jarid1a*) and in translational control (*Btg2, Paip2a*). Coordinated regulation of these targets underlies miR-132-dependent modulation of *Period* gene expression and clock entrainment. Our findings identify miR-132 as an orchestrator of the processes of chromatin remodeling and protein translation within the mammalian master clock, thereby fine-tuning clock entrainment.

RESULTS

Computational analyses of miR-132-predicted targets reveal a high abundance of chromatin- and translation-associated genes

Microarray analyses of miRNA targets (23) have revealed that miRNAs regulate a large number of genes in a tissue-specific

fashion. In addition, a wide variety of *in vivo* studies (24–26) have hinted at miRNAs being regulators of specific biological processes/pathways in defined tissues via coordinated regulation of genes with common functions. These studies led us to hypothesize that within the SCN miR-132 tightly regulates one or more classes of functionally related genes, which in turn may mediate the effects of miR-132 on light-induced clock entrainment. Indeed, the current study was motivated by the initial observation that a fair number of miR-132-predicted targets appeared to be involved in the processes of chromatin remodeling and translational control. In order to test rigorously the hypothesis that the miR-132 target set is enriched for genes falling into these two functional categories, we performed a computational analysis upon the functional annotations of the predicted gene targets. Predicted microRNA targets were obtained from TargetScan (release 5.1, April 2009) (27). TargetScan predicts biological targets of miRNAs via the presence of conserved sites that match the seed region of the miRNA. Thus, to avoid confounding effects due to sequence conservation and the associated emergence of functions along evolution, we restricted the analysis to the set of miRNAs belonging to the same family as miR-132, i.e. conserved across most vertebrate species. From these, we further focused on microRNAs with 50 or more predicted conserved targets. Using the Gene Ontology (GO) annotations from the Mouse Genome Informatics (MGI) database (GO Reference MGI), we selected two GO terms (including all of their children) that adequately represent our two categories of interest: chromatin remodeling and translational control. For each miRNA, we measured the frequency of its conserved targets that are annotated with GO terms 'chromatin modification' (GO:0016568) and/or 'chromatin assembly or disassembly' (GO:0006333) or any of their children terms in the ontology. The results show that miR-132 is highly enriched for conserved target genes that are involved in chromatin function (Fig. 1A and Supplementary Material, Table S1). Out of 78 miRNAs analyzed, miR-132 had the third highest percentage of chromatin-related targets. Interestingly, miR-194, which shares a significant overlap of predicted targets with miR-132 as a result of the high similarity in their seed sequences, had the highest percentage of chromatin-related targets. An analogous study was carried out for occurrences of the GO term 'translation' (GO: 0006412) and its children terms in the ontology. miR-132 is ranked eighth among 78 miRNAs, indicating that translation-associated genes are more abundant than average for miR-132 (Fig. 1B and Supplementary Material, Table S2). The outcome of our computational analyses supports the initial observation that the target gene set of miR-132 is enriched for genes implicated in chromatin function and protein translation.

The 3′UTRs of the chromatin remodeling factors, *Mecp2*, *Ep300* and *Jarid1a*, and the translation control regulators, *Btg2* and *Paip2a*, are direct targets of miR-132 *in vitro*

Next, we selected five putative miR-132 target genes (*Mecp2*, *Jarid1a*, *Ep300*, *Btg2* and *Paip2a*) falling into either the 'chromatin' or the 'translation' groups for further analysis. These targets were chosen because: (1) preliminary real-time-polymerase chain reaction (RT-PCR) experiments as well as published observations (28,29) indicate their expression in the murine SCN; (2) existing literature suggests that the gene itself may have a potential role in the clock timing process (6,29); and/or (3) existing literature has established a functional link between the miR-132 target and another gene, the latter having previously been implicated in the clock timing process (e.g. MeCP2 and CREB (30), JARID1A and H3K4Me3 (31)).

To determine whether miR-132 targets the expression of *Mecp2*, *Ep300*, *Jarid1a*, *Btg2* and *Paip2a* via the predicted miR-132 response elements (MREs) within their 3′UTRs (Fig. 1C), we generated firefly luciferase reporter constructs bearing the full-length wild-type 3′UTR of the various genes, or a full-length mutant 3′UTR containing a 7-bp deletion of the seed sequence. In the case of *Paip2a*, because the 7-bp deletion resulted in a significant deterioration of basal firefly luciferase activity relative to the wild-type construct (data not shown), we opted for a mutant reporter construct that carried a 2-nucleotide mismatch within the seed sequence. Neuro-2a cells were transfected with each of the reporter constructs in combination with a synthetic miR-132 'mimic' (double-stranded ∼22-bp RNA oligonucleotides that mimic endogenous mature miRNA function) or a microRNA Negative Control (dsRNA oligonucleotides that have no complementarity to any known sequence in the human, rat or mouse genome). As a control, we also transfected Neuro-2a cells with the backbone firefly luciferase construct pGL3-Control, which lacks a miR-132 MRE site, in combination with the miR-132 mimic or the microRNA Negative Control. In this case, co-transfection of the miR-132 mimic, but not the microRNA Negative Control, caused a subtle (∼5–10%) reduction in luciferase activity, which we attributed as a non-sequence-specific effect of miR-132 overexpression *in vitro*. Most importantly, the wild-type 3′UTRs of all genes examined were significantly repressed by the miR-132 mimic, with a range of repression between 28 and 50% (Fig. 1D). In all cases except for *Jarid1a*, the effects of the miR-132 mimic were abolished by the mutation of the seed site (Fig. 1D). For *Jarid1a*, which bears two putative miR-132 MREs within its 3′UTR, mutation of the first MRE (site 1), but not the second (site 2), abolished the repressive effects of the miR-132 mimic (Fig. 1D).

To examine whether miR-132 regulates the expression of MeCP2, p300, JARID1A, BTG2 and PAIP2A at the protein level, we inhibited the function of endogenous mature miR-132 in Neuro-2a cells with a mouse miR-132 hairpin inhibitor and assessed protein abundance via western blotting 24 h post-transfection (Fig. 1E; see also Supplementary Material, Fig. S1 for antibody validation). Compared with cells that had been transfected with a negative control inhibitor (i.e. inhibitor with unmatched mouse, human or rat sequence), miR-132 inhibitor-transfected cells expressed greater levels of all five candidate target genes (Fig. 1E). Collectively, our data indicate that the protein expression of these predicted targets of miR-132 are repressed *in vitro* by miR-132 via specific miR-132 MRE sequences.

Upregulation of miR-132 in the SCN attenuates light-induced clock resetting

Our *in vitro* results prompted us to ask whether the expression of MeCP2, p300, JARID1A, BTG2 and PAIP2A within the

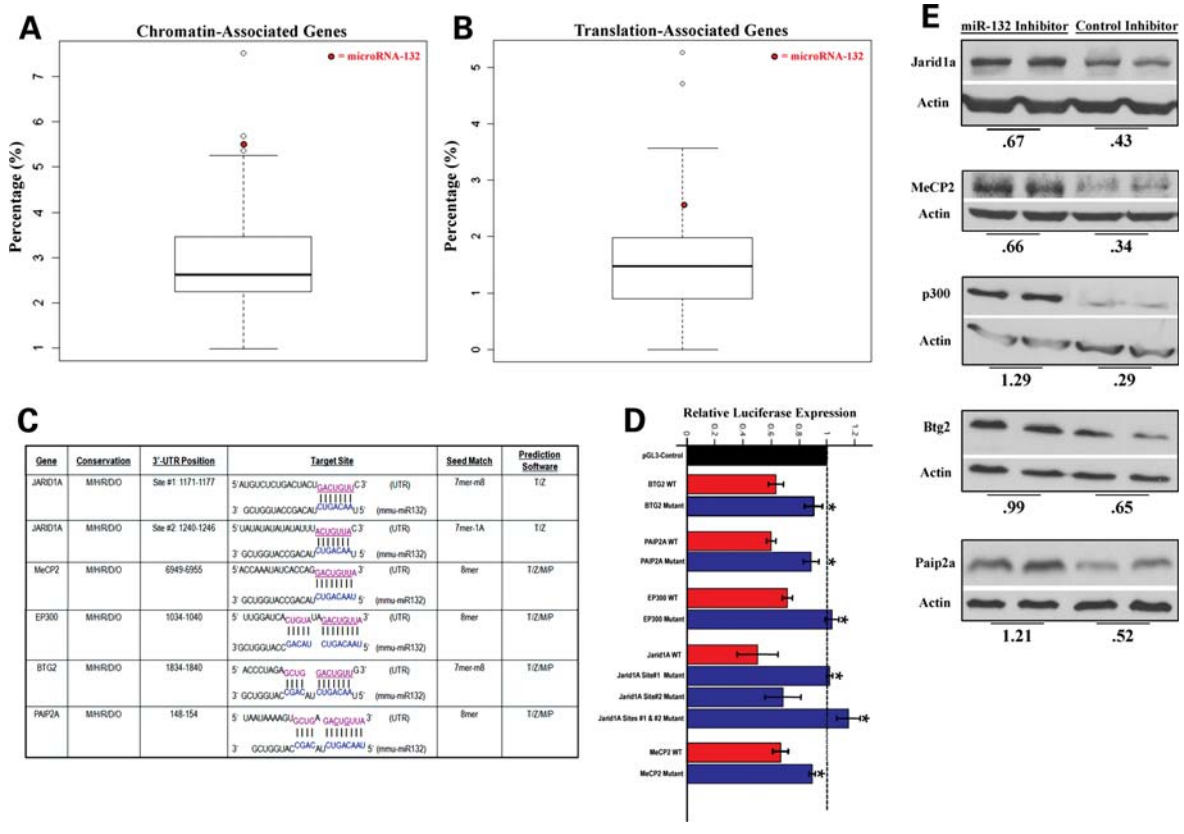

Figure 1. Computational analyses on functional annotations and *in vitro* validation of predicted targets of miR-132. (**A**) Box plot of the percentage distribution of predicted microRNA targets with putative chromatin-related functionality. The red dot shows miR-132 (5.5%) as an extreme point. (**B**) Box plot of the percentage distribution of predicted microRNA targets that are involved in translation-associated regulation. The red dot shows miR-132 (2.5%) well above the upper quartile (1.96%). (**C**) Table of miR-132 target sites within the 3′UTRs of murine *Jarid1a*, *Mecp2*, *Ep300*, *Btg2* and *Paip2a*. Site conservation across species: M, mouse; H, human; R, rat; D, dog; O, opossum. Position of predicted miR-132 target sites within the 3′UTR (first nucleotide after the stop codon is denoted as position 1). Target site: alignment of the 3′UTR and miR-132. Nucleotides in purple and blue indicate complementarity. With the exception of *Paip2a*, mutant 3′UTRs were generated by deletion of the underlined nucleotides. For *Paip2a*, the underlined nucleotides were mutated via a C → G or G → C conversion. Predicted as a target of mmu-miR-132 based on the following target prediction websites: T, TargetScan; Z, MirZ; M, miRanda; P, PicTar. (**D**) miR-132 mediates 3′UTR-dependent repression of luciferase reporter activity via specific miR-132 target sites. Neuro-2a cells were transfected with luciferase reporter constructs carrying the full-length wild-type (WT) or mutant 3′UTRs of *Btg2*, *Paip2a*, *Ep300*, *Jarid1a* and *Mecp2* in combination with synthetic miR-132 Mimic or a miRNA Mimic Negative Control. Renilla luciferase activity was used as an internal transfection control and was used to normalize raw firefly luciferase (FL) values. Control transfections using the backbone pGL3-Control vector (no 3′-UTR) in combination with miR-132 Mimic, miRNA Mimic Negative Control, or pcDNA3.1 empty vector were used to assess non-specific effects of miR-132 on a reporter construct that lacks a miR-132 target site, as well as potential effects of the Negative Control on luciferase activity. Values on the *x*-axis indicate relative luciferase activity = $(UTR_{mimic}/UTR_{neg})/[(pGL3\text{-}C_{mimic})/(pGL3\text{-}C_{neg})]$, where UTR and pGL3-C denote samples transfected with the 3′UTR reporter or the backbone pGL3-Control vector, respectively. Black bar denotes control transfection using pGL3-Control and is normalized to 1. Error bars represent the standard deviation from triplicate determinations of a single representative experiment. Consistent results were obtained from three independent experiments. In all cases, the relative luciferase activities of constructs bearing WT 3′UTRs were significantly reduced relative to control (black bar), and, with the exception of site #2 within the *Jarid1a* 3′UTR, mutation of the predicted target sites provided nearly complete rescue. $^{*}P < 0.05$ versus WT 3′UTR (two-tailed Student's *t*-test and one-way ANOVA). (**E**) JARID1A, MeCP2, p300, BTG2 and PAIP2A protein levels in Neuro-2a cells following transient knockdown of endogenous miR-132 expression as determined by western blotting. Neuro-2a cells were transiently transfected with miR-132 hairpin inhibitors (lanes 1 and 2) to knock down miR-132 expression, or a microRNA hairpin inhibitor negative control (lanes 3 and 4). Twenty-four hours post-transfection, cells were harvested, and protein lysates were analyzed by western blotting. Actin expression served as the loading control. Values presented below the blot represent the mean relative abundance of the protein examined, normalized to actin expression, for each transfection condition. Three independent experiments were performed, and similar results were obtained.

murine SCN is regulated by miR-132. For this purpose, we developed a novel, tetracycline (tet)-inducible miR-132 transgenic mouse strain (denoted simply as miR-132 mice). The sequence of the rat miR-132 precursor (pre-miR-132), which is highly conserved in multiple metazoan species, was cloned into a bidirectional tet-responsive promoter, along with a destabilized version of the marker protein enhanced cyan fluorescent protein (ECFP) (i.e. carrying a proline-, glutamic acid-, serine- and threonine-rich (PEST) domain) as the second transgene (Fig. 2A). This transgenic strain was crossed with the *Camk2α*-tTA activator line (32), which has previously been shown to drive transgenic expression in the forebrain under doxycycline-free conditions, to produce *Camk2α*-tTA::miR-132 double transgenic mice (hereafter referred to as tTA::miR-132). By quantitative RT-PCR, we confirmed that the abundance of mature miR-132 is upregulated in the SCN of double transgenic mice from 2.7- to 7.5-fold relative to non-transgenic controls, depending on the

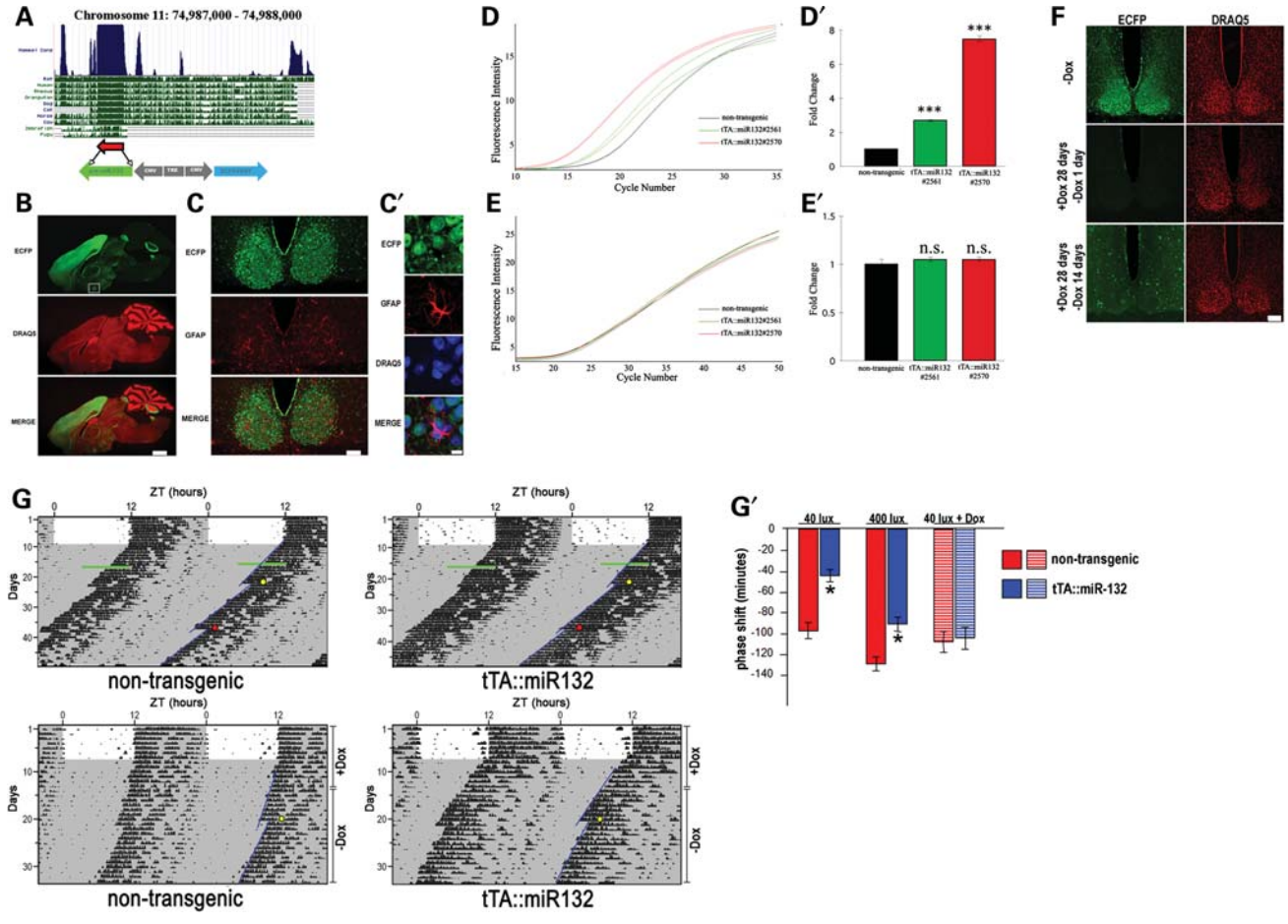

Figure 2. miR-132 transgenic mice exhibit attenuated light-induced clock resetting of behavioral rhythms. (**A**) Conservation of miR-132 across species. Position of murine (mmu-)miR-132 gene on chromosome 11 (top). Alignment scores are indicated by green bars in the conservation track of the species listed. Red arrow immediately below the conservation tracks indicates the position of the miR-132 stem-loop precursor sequence. (Bottom) Transgene design. The pre-miR-132 sequence (green arrow) and the ECFP-PEST minigene cassette (blue arrow) were cloned in opposite orientations flanking a bidirectional tet-responsive promoter. CMV, minimal CMV promoter; TRE, tet-responsive element. (**B**, **C**) ECFP transgenic expression in the brains of *Camk2α*-tTA::miR-132 transgenic mice. (**B**) Sagittal and (**C**, **C'**) coronal SCN sections were processed for ECFP immunoreactivity using a goat polyclonal anti-GFP (green) antibody. In (B), sections were counterstained with the nuclear marker, DRAQ5 (pseudocolored in red). Scale bar = 1 mm. In (C, C'), sections were co-labeled for GFAP immunoreactivity (red) and counterstained with DRAQ5 (blue). Note the lack of co-localization in (C'). Scale bar = 50 μm (for C) and 10 μm (for C'). The abundance of (**D**) mature miR-132 and (**E**) mature miR-219 in the SCN of non-transgenic (black line) and tTA::miR-132 transgenic (green and red lines) mice was determined by ABI Taqman® miRNA qPCR analysis. Raw data are presented as fluorescence intensity versus number of PCR cycles. Two independent miR-132 founder lines, #2561 and #2570, were examined. SCN tissues from three mice were pooled for each sample, from which quadruplicate determinations were made. Quantitation of (**D'**) miR-132 and (**E'**) miR-219 abundance from (D) and (E), respectively. Data are quantified and presented as relative fold change, in which values for non-transgenic controls are set arbitrarily as 1. Error bars denote SEM of quadruplicate determinations. $^{***}P < 0.001$, n.s. = non-significant versus non-transgenic control (one-way ANOVA). (**F**) Assessment of Dox-mediated transgene silencing in tTA::miR-132 mice. Adult mice were fed Dox-containing rodent chow (6 mg/g food) for 28 days and then returned to a regular diet lacking Dox for an additional 14 days. Three treatment groups were examined for ECFP transgene expression: (top) Dox-naïve mice (−Dox) and Dox-fed mice that were killed (middle) 1 day after cessation of Dox treatment (+Dox 28 days/−Dox 1 day), or (bottom) 14 days after cessation of Dox treatment (+Dox 28 days /−Dox 14 days). Brain sections were processed for ECFP (green) immunoreactivity using a polyclonal anti-GFP antibody, and counterstained with DRAQ5 (pseudocolored in red). Scale bar = 100 μm. $n = 5$ mice per condition. (**G**, top panels) Representative double-plotted actograms of wheel-running activity of non-transgenic (left) and tTA::miR-132 transgenic (right) mice maintained under doxycycline-free conditions. Mice were stably entrained to a fixed 12 h:12 h light–dark (LD) cycle prior to release into constant darkness (DD). After 2 weeks in DD, mice received a single, 15-min light pulse of 40 lux intensity (yellow circle) at CT 15, and returned to DD. After 15 days, mice received a second light pulse of higher intensity (red circle: 15 min, 400 lux) at CT 15, and returned to DD for an additional 2 weeks. Note that tTA::miR-132 transgenic mice exhibit smaller light-induced phase shifts at both light intensities, compared with non-transgenic controls. Periods of darkness are shaded in gray. Activity onsets are indicated by blue lines. The *x*-axis indicates the Zeitgeber (ZT) time of the initial 12 h:12 h light–dark cycle (100 lux during the L portion). The *y*-axis indicates the *n*th day of the study. Missing activity data on day 17 (green bars) were due to computer malfunction. (**G**, bottom panels) Representative double-plotted actograms of non-transgenic (left) and tTA::miR-132 transgenic (right) mice that had been maintained on a Dox diet (6 mg/g food) during adulthood for 4 weeks in order to 'turn off' miR-132 transgene expression. Mice were returned to regular, Dox-free rodent chow 1 week prior to exposure to a single, 15-min light pulse of 40 lux intensity (yellow circle) at CT 15. Note that doxycycline treatment restored the magnitude of light-induced phase shifts of tTA::miR-132 transgenic mice to the level of non-transgenic controls. (+Dox) Period of Dox feeding; (−Dox) Dox-free conditions. (**G'**) Quantitation of the effects of miR-132 transgenic expression and doxycycline treatment on CT 15 light-induced phase shifts. Values are presented as mean ± SEM phase shift (in min). Negative values indicate phase delays. $n = 10–14$ per group. $^{*}P < 0.05$ versus same-treated non-transgenic control (two-tailed Student's *t*-test).

miR-132 founder line examined (Fig. 2D and D'). As a control, we found no difference in the levels of miR-219, another miRNA that is expressed in the SCN, between the two genotypes (Fig. 2E and E'). Furthermore, we showed that the ECFP marker is expressed primarily in the forebrain, although moderate-to-strong expression was also observed in other brain regions such as the inferior colliculus, cerebellum, area postrema and ventral brainstem (Fig. 2B). ECFP is expressed robustly in the majority of SCN neurons (>90%) and is, for the most part, not expressed by glial cells within the SCN (Fig. 2C and C'). The data presented in the following sections were obtained from the 'high expressor' founder line #2570, but the phenotype of the 'low expressor' line #2561 was qualitatively similar.

To validate the utility of our miR-132 transgenic mice as a model to probe the function of endogenous miR-132, we first characterized their circadian behavior and compared it with our published work with miR-132-antagomir-treated mice (19). Both non-transgenic and tTA::miR-132 mice were able to entrain stably to a full photoperiod of 12 h light:12 h dark (LD 12:12) (Fig. 2G, top), and both remained rhythmic in behavior upon subsequent release into conditions of constant darkness (DD) for 2 weeks. There was a tendency toward a slightly shortened circadian period length in the tTA::miR-132 mice compared with non-transgenic littermate controls [period (h) of non-transgenic versus tTA::miR-132 mice: 23.81 ± 0.05 versus 23.67 ± 0.03, $P = 0.055$]. These data indicate that transgenic expression of miR-132 does not compromise the generation and maintenance of circadian rhythms, or stable entrainment to a full photoperiod.

We further examined the role of miR-132 in light-induced clock entrainment using a different behavioral paradigm that gauges the responsiveness or sensitivity of the clock to light administered at specific circadian times (CTs). After 2 weeks in DD, mice received a 15-min light pulse of medium intensity (40 lux) in the early night (CT 15) (Fig. 2G, top panels, yellow circle). In non-transgenic mice, this light treatment resulted in a mean phase delay of -98 ± 7.7 min (Fig. 2G, top, and 2G'). Notably, light (40 lux)-induced phase delays were greatly reduced in tTA::miR-132 mice (-45 ± 5.8 min, $P < 0.01$). The attenuated phase-delaying response exhibited by tTA::miR-132 mice was not due to reduced sensitivity of the clock to light, because a second light pulse (15 min, CT 15) of high intensity (400 lux: red circle), administered 2 weeks later also resulted in a diminished phase-shifting response in tTA::miR-132 mice compared with non-transgenic littermate controls [phase delay (min) of non-transgenic versus tTA::miR-132 mice to 400 lux light pulse: -130 ± 6.9 versus -92 ± 6.7, $P < 0.05$] (Fig. 2G, top and G'). Moreover, the circadian behavior of tTA and miR-132 single transgenic mice were indistinguishable from that of non-transgenic controls, arguing against the possibility of tTA expression *per se* or potential disruptive effects of miR-132 transgene integration as the underlying cause of the reduced phase-shifting effects of light in tTA::miR-132 mice.

The *Camk2a* promoter is active during mouse embryogenesis (32). Therefore, to rule out the possibility that the reduced phase delays exhibited by the tTA::miR-132 mice resulted from an irreversible effect of miR-132 overexpression during development, we fed adult mice a Dox-containing diet (6 mg/g rodent chow) *ad libitum* for 4 weeks to silence transgenic expression. During this time, mice were maintained in wheel cages under a fixed LD schedule. After the third week of Dox feeding, mice were released into DD, and 1 week after return to regular rodent chow (no Dox), mice received a brief light pulse (15 min, 40 lux) at CT 15 (Fig. 2G, bottom panels). Non-transgenic as well as tTA::miR-132 mice that were both fed a Dox diet showed light-induced phase delays that were statistically indistinguishable [phase delay (min) of non-transgenic versus tTA::miR-132 mice: -109 ± 10.1 versus -106 ± 10.5, $P > 0.05$] (Fig. 2G, bottom panels and 2G'). By immunofluorescent staining, we verified that the 4-week Dox regimen completely turned off ECFP transgene expression in the SCN of tTA::miR-132 mice and that 2 weeks after return to *ad libitum* feeding on regular rodent chow, transgene expression in the SCN had not as yet reactivated, except for a few isolated cells (Fig. 2F).

Collectively, the data indicate that upregulation of miR-132 expression in the SCN of adult mice attenuates light-induced resetting of behavioral rhythms. These data are consistent with our previously published work showing that miR-132 knockdown in the SCN potentiates light-induced phase-shifting (19) and establishes the utility of our miR-132 transgenic mice as a model to probe endogenous miR-132 function.

miR-132 affects the expression of endogenous MeCP2, p300, JARID1A, BTG2 and PAIP2A

Next, using the tTA::miR-132 mice, we analyzed the expression of MeCP2, p300, JARID1A, BTG2 and PAIP2A in the murine SCN upon miR-132 overexpression.

JARID1A (Jumonji, AT-rich interactive domain 1A) and other members of the JARID1 family are histone demethylases that specifically remove a methyl group from lysine 4 of the tri (H3K4Me3)- and di (H3K4Me2)-methylated forms of histone H3 (33). As part of the 'histone code' (34), the H3K4Me3 and H3K4Me2 marks are generally associated with sites of active transcription. H3K4-Me3/Me2 may facilitate transcription by recruiting additional chromatin remodeling factors or histone modifying enzymes, or impeding the binding of transcriptional repressors. Although there are no reports that directly implicate JARID1A in circadian clock processes, the promoter of the clock-regulated gene, *Dbp*, exhibits circadian rhythms in H3K4 trimethylation (31). As a first step toward this end, we found that JARID1A protein is expressed in the murine SCN at CT 16, a time when endogenous miR-132 expression is at its nadir (Fig. 3D and D'). Furthermore, overexpression of miR-132 resulted in diminished levels of JARID1A in the SCN (Fig. 3D, D' and F). As expected, the decreased expression of JARID1A in tTA::miR-132 transgenic SCN at CT 16 was accompanied by a concomitant increase in H3K4Me3 immunoreactivity (Supplementary Material, Fig. S2). This heightened expression in H3K4Me3 within the SCN may be alternatively explained by an upregulation of histone methyltransferase activity in the transgenics. However, we examined the expression of two methyltransferases, DNMT3A and SMYD2, and found either no expression in the SCN of non-transgenic and tTA::miR-132 mice (in the case of DNMT3A) or comparable levels in the SCN regardless of genotype (in the case of SMYD2) (data not shown).

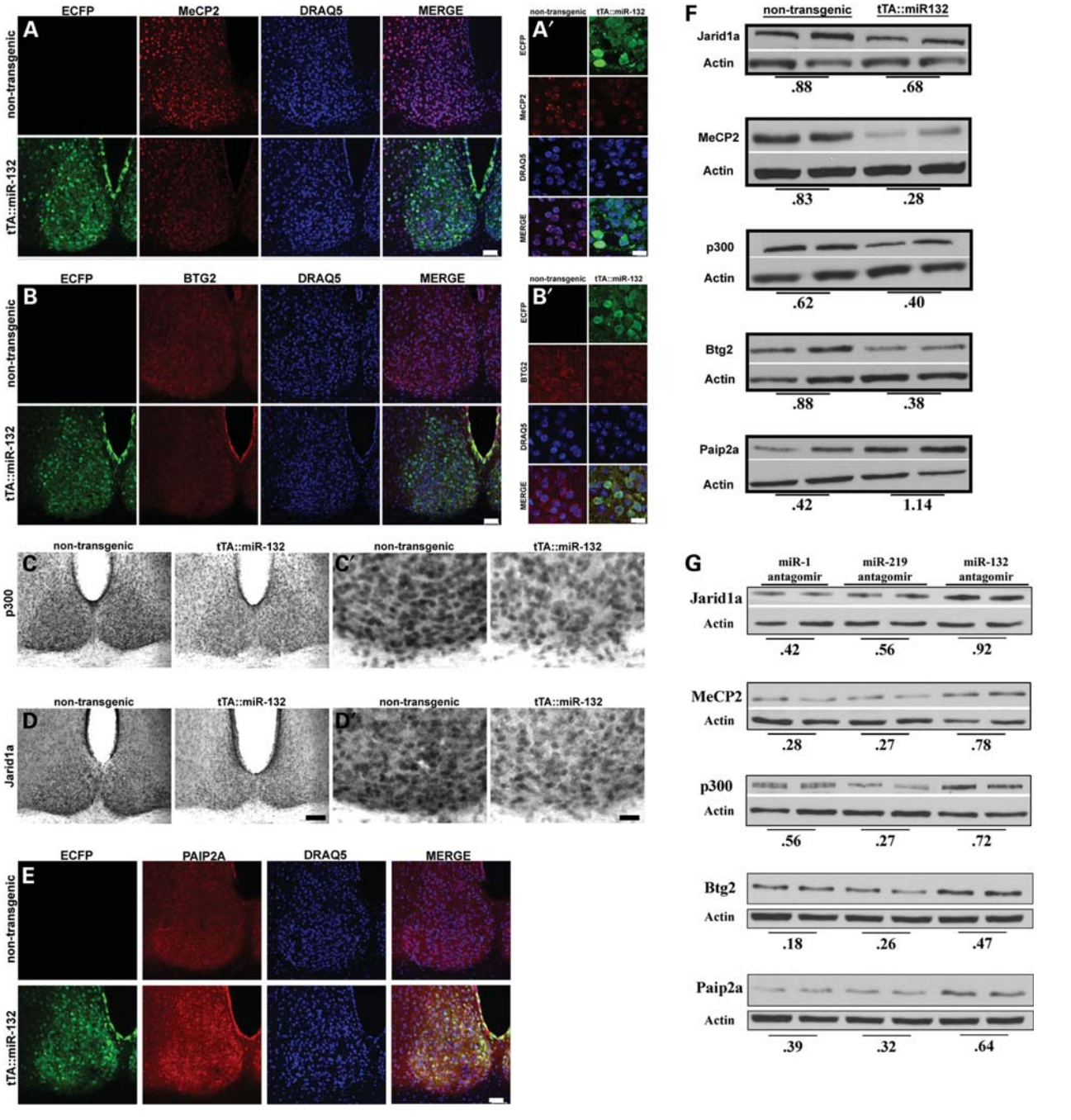

Figure 3. miR-132 regulates the expression of MeCP2, p300, JARID1A, BTG2 and PAIP2A in the SCN. MeCP2, BTG2 and PAIP2A protein expression in the SCN of tTA::miR-132 transgenic mice and non-transgenic controls at CT 16. SCN tissue from non-transgenic (top row) and tTA::miR-132 transgenic (bottom row) mice was harvested at CT 16 and analyzed for expression of (**A**) MeCP2, (**B**) BTG2 and (**E**) PAIP2A by indirect immunofluorescence (red). Transgenic expression was confirmed by co-detection of ECFP (green). Sections were counterstained with the nuclear marker DRAQ5 (blue). Merged images are presented in the rightmost columns. Scale bars = 50 μm. (**A'**, **B'**) Expression of (**A'**) MeCP2 and (**B'**) BTG2 in the retinorecipient region of the SCN, the ventrolateral aspect, is presented in higher magnification. Note the heterochromatic distribution of MeCP2 as well as the cytoplasmic distribution of BTG2. Scale bars = 5 μm. Immunohistochemical detection of (**C**) p300 and (**D**) JARID1A protein expression in the SCN of tTA::miR-132 transgenic mice and non-transgenic controls at CT 16. Scale bars = 100 μm. Expression of (**C'**) p300 and (**D'**) JARID1A in the ventrolateral SCN is given in higher magnification images. Scale bars = 20 μm. For (A) to (E), $n = 6$ mice per genotype and representative images were chosen. (**F**) MeCP2, BTG2, p300, JARID1A and PAIP2A protein expression in the SCN of tTA::miR-132 transgenic mice (lanes 3 and 4) and non-transgenic controls (lanes 1 and 2) as determined by western blotting. Actin expression served as loading control. Values presented below each blot represent the mean relative abundance of the protein examined, normalized to actin expression, for each genotype. $n = 4$ mice per genotype, grouped in pools of two. The experiment was repeated three times with separate pooled samples, and similar results were obtained. (**G**) The effect of antagomir-mediated knockdown of endogenous miR-132 on the expression of MeCP2, BTG2, p300, JARID1A and PAIP2A in the murine SCN. C57Bl/6J mice were dark-adapted for 2 days and then infused with antagomirs (100 μM, 3 μl) against miR-132, miR-1 or miR-219 into the lateral ventricles at CT 15. The following day, mice received a brief light pulse (15 min, 100 lux) at CT 15, and 8 h later (CT23) SCN tissue was harvested for analysis of protein expression by western blotting. Actin expression served as the loading control. Values presented below each blot represent the mean relative abundance of the protein examined, normalized to actin expression, for each genotype. $n = 10$ mice per treatment condition, grouped in pools of two.

The role of p300 (E1A-binding protein) and its homolog, CBP (CREB-binding protein), in transcriptional regulation has been extensively documented (35). These factors interact with a multitude of transcription factors, including CREB, as well as components of the general transcriptional machinery, to activate or repress gene transcription. Additionally, both p300 and CBP have been implicated in chromatin remodeling, as they possess intrinsic acetyltransferase activity, and have been shown to acetylate histones and other proteins. The observation that p300 physically associates with CLOCK and promotes CLOCK/BMAL1-mediated transcription in the liver (6), together with evidence that the promoters of several core clock genes exhibit circadian rhythms in histone H3 acetylation, provides support for a role of p300 in circadian clock function in peripheral oscillators. With this in mind, we examined whether p300 expression in the SCN was under miR-132 regulation. Using immunohistochemical (Fig. 3C and C') as well as western blot (Fig. 3F) approaches, we noted a ∼30% reduction in p300 protein levels in the SCN of tTA::miR-132 mice compared with non-transgenic controls at CT 16, although the number of p300-expressing cells was comparable between the two genotypes.

Methyl CpG-binding protein 2 (MeCP2) is a nuclear protein that has the ability to bind to methylated CpG dinucleotides commonly located within transcribed regions of the genome. Although early observations suggested that MeCP2 functioned as a silencer of gene transcription (36), emerging evidence points to additional roles for MeCP2 within the nucleus, including chromatin compaction, alternative splicing and transcriptional activation (30,37). Functional interactions between MeCP2 and CREB, a key intermediate in light-induced clock entrainment, have been reported (30). Interestingly, patients suffering from the autism-spectrum disorder, Rett syndrome, which is caused by mutations of the *MECP2* gene, exhibit disruptions in their circadian rhythms (38), suggesting a possible, direct link between MeCP2 and clock function. Notably, we found that levels of MeCP2 within the SCN at CT 16 were strongly diminished by miR-132 transgene expression (Fig. 3A). Higher magnification reveals the hallmark heterochromatic localization of MeCP2, with reduced levels seen in the heterochromatic foci of cells overexpressing the transgene (Fig. 3A'). Western blot analysis using SCN extracts revealed a 65% reduction in total MeCP2 expression in miR-132 transgenic SCN compared with non-transgenic controls (Fig. 3F).

B-cell translocation gene 2 (BTG2) was recently shown to bind to POP2/CAF1, a subunit of the CCR4/POP2 deadenylase complex that is responsible for shortening of the poly(A) tail, the rate-limiting step in mRNA turnover (39). One study demonstrated that BTG2 induces mRNA decay by increasing the rate of POP2/CAF1-mediated deadenylation (39). Recent evidence suggesting the importance of mRNA degradation in modulating circadian rhythms of *mPer2* expression (40) raises the possibility for a role of BTG2 in circadian clock regulation. By immunofluorescent labeling, we found that BTG2 levels were attenuated in the SCN of tTA::miR-132 mice compared with non-transgenic controls (Fig. 3B and B'). A similar downregulation in BTG2 expression (55% reduction) was observed via western blot analysis (Fig. 3F).

Polyadenylate-binding protein-interacting protein 2 (PAIP2A) is a potent suppressor of eukaryotic translation. EIF4G, a component of the translation initiation complex that binds to the 5′-cap of mRNA, interacts physically with polyadenylate-binding protein (PABP) that is bound to the poly(A) tail, leading to circularization of the mRNA and enhanced translation efficacy (41). PAIP2A inhibits translation by disrupting the interaction between the poly(A) tail and PABP (42). Thus far, there has been no characterization of PAIP2A in clock mechanisms. However, its functional partner, PABP-C1 (PABP, cytoplasmic 1) exhibits circadian rhythms of gene expression in the liver (43) and is a potential target of CREB transcription (unpublished data). Furthermore, a recent study showed that the mTOR signaling pathway, a key regulator of translation, is induced by light in the SCN (17), suggesting a role of translational regulation in photic entrainment. Contrary to the results from the 3′UTR reporter assays and endogenous miR-132 inhibition in Neuro-2a cells, we noted an unexpected augmentation of PAIP2A levels in the SCN of tTA::miR-132 mice, relative to non-transgenic controls, at CT 16 (Fig. 3E). Western blot analysis confirmed a 2.7-fold increase in PAIP2A expression in miR-132 transgenic SCN relative to non-transgenic controls (Fig. 3F). One possibility is that constitutive and long-term overexpression of miR-132 in the SCN, within a certain cellular context, alters other gene-regulatory networks that have secondary effects on PAIP2A expression, for example, at the level of gene transcription. These secondary effects may mask the direct effects of miR-132 on PAIP2A expression via the miR-132 MRE within the *Paip2a* 3′UTR.

Lastly, using an *in vivo* knockdown approach, we examined the effect of endogenous miR-132 on the expression of these five targets within the SCN. C57Bl/6J (wild-type) mice received an intracerebroventricular infusion of the miR-132 antagomir at CT 15, and 24 h later treated with a brief light pulse (15 min, 100 lux) at CT 15 in order to induce endogenous miR-132 expression (19). Target protein expression in the SCN 8 h post-light treatment was examined by western blotting. Compared with mice that had received infusions of either miR-219 or miR-1 antagomirs, or vehicle control, miR-132 antagomir-infused mice exhibited an upregulation of MeCP2, p300, JARID1A, BTG2 and PAIP2A protein levels in the SCN (Fig. 3G and Supplementary Material, Fig. S3). Our results for MeCP2 and p300 are consistent with previous reports demonstrating augmented expression in primary neuronal cultures (44) and virus-infected endothelial cells (45), respectively, following miR-132 knockdown. Also noteworthy is the observation that PAIP2A levels were increased in the SCN of miR-132 antagomir-infused mice (Fig. 3G), in contrast with our transgenic results.

Thus, using a combination of 3′UTR reporter assays as well as *in vivo* gain-of-function and *in vitro* and *in vivo* loss-of-function approaches, we demonstrate that JARID1A, p300, MeCP2, BTG2 and PAIP2A are bona fide targets of miR-132. In the case of four of these targets (PAIP2A being the exception), this manifests in reduced steady-state levels of the target protein in the SCN of an intact mouse that overexpresses miR-132. Overexpression of miR-219 in the SCN using a tTA::miR-219 transgenic mouse model had no effect on the expression of JARID1A, p300, MeCP2, BTG2 or

PAIP2A—as none of these bear a predicted miR-219 MRE in their 3′UTRs, arguing that the changes in target expression that were observed in tTA::miR-132 mice were indeed sequence-specific effects of miR-132 (Supplementary Material, Fig. S4). However, potential alterations in genetic networks in the tTA::miR-132 transgenic SCN may secondarily influence the expression of the *Paip2a* gene, to an extent that these effects may mask the MRE-mediated effects of miR-132 on PAIP2A expression.

miR-132 target genes and their downstream effectors are acutely induced by light

Our *in vivo* results establish MeCP2, p300, JARID1A, PAIP2A and BTG2 as bona fide targets of miR-132 within the SCN and raise the possibility that these targets may play a role in mediating the suppressive effects of miR-132 on light-induced clock resetting. Indeed, these targets may themselves be regulated by light, if they play a role in modulating the responses of the SCN to photic stimulation. As a first step toward characterizing their roles in the SCN, we examined the light-dependent expression or activity (e.g. as indicated by specific post-translational modifications) of these targets or their downstream effectors. Mice were subjected to a brief light pulse (15 min, 40 lux) at CT 15, and SCN tissue was harvested either 15 min or 2 h later to determine changes in post-translational modifications or total protein abundance, respectively. Phosphorylation of MeCP2 at residue Serine 421 (pS421), previously shown to be induced by neuronal activity and is required for derepression of *Bdnf* transcription (28), is robustly induced in the ventrolateral SCN in response to light (Fig. 4A, A' and E). Similarly, light elicited a pronounced elevation in the expression of H3K4Me3, the direct substrate of JARID1A, suggesting the possibility that light has an acute suppressive effect on JARID1A demethylase activity (Fig. 4B, B' and E). As an aside, following light exposure, we also noted rapid induction of the tri-acetylated form of the replacement histone H2A.Z at lysines 4, 7 and 11 (K4 + K7 + K11) (Supplementary Material, Fig. S5), a marker of transcriptionally active genes (46). Thus, it appears that light evokes rapid changes in chromatin architecture within the SCN that, together, favor a transcriptionally permissive state. Lastly, levels of BTG2 (Fig. 4C, C' and E) as well as PAIP2A proteins (Fig. 4D, D' and E) in the SCN were significantly induced 2 h following photic stimulation. Collectively, our results indicate that the miR-132 targets examined, or the pathways that are directly regulated by the target, are themselves acutely induced in the SCN in response to light, arguing that these targets play a role in modulating light-induced clock resetting.

Circadian and light-inducible expression of *Period* genes are dampened in the SCN of miR-132 transgenic mice

Next, we focused on the potential involvement of miR-132 in core clock timing mechanisms. To this end, we examined the circadian profile of PER1 and PER2 protein expression in the SCN of tTA::miR-132 mice and non-transgenic controls. Consistent with previous reports, the peak and nadir of PER1 and PER2 protein expression in the SCN of non-transgenic (i.e. wild-type) mice were reached during the early subjective night (CT 14) and late subjective night (CT 22)/early subjective day (CT 2), respectively (Fig. 5A, B, E and F). Compared with non-transgenic controls, tTA::miR-132 mice exhibited a marked reduction in the amplitude of PER1 rhythms in the SCN (Fig. 5A and E). The dampened rhythm was due largely to a decrement in PER1 abundance during the peak (CT 10–14), rather than elevated expression during the nadir (Fig. 5E). The phasing of PER1 expression in the SCN was comparable between non-transgenic and tTA::miR-132 mice. In contrast, miR-132 overexpression in the SCN had no significant effect on PER2 protein rhythms (Fig. 5B and F).

Numerous studies have shown a strong correlation between phase shifting of behavioral rhythms and induction of *Per1* and *Per2* expression in the SCN following nocturnal light exposure (47,48). To examine light-inducible expression of PER1 and PER2 in the SCN, tTA::miR-132 mice and non-transgenic controls were administered a brief light pulse (15 min, 40 lux) at CT 15 and killed 4 h later for determining PER1 and PER2 levels. Consistent with previous studies (49), light exposure during the early subjective night significantly increased the number of PER1- and PER2-immunoreactive (IR) cells in the SCN of non-transgenic (wild-type) mice relative to dark controls (Fig. 5C, D, G and H). There was a modest but significant increase in the number of PER1-IR cells in tTA::miR-132 transgenic SCN in response to photic stimulation, relative to dark controls (Fig. 5C and G). However, the number of PER1-IR nuclei after a light pulse in the transgenics was merely one-half of that observed in non-transgenic controls (Fig. 5C and G). Light exposure produced an incremental increase in the abundance of PER2-IR cells in the SCN of tTA::miR-132 mice relative to dark controls (Fig. 5D and H). Indeed, the number of PER2-IR nuclei in light-pulsed tTA::miR-132 mice was markedly fewer than that observed in light-pulsed non-transgenic controls (Fig. 5D and H). Together, these data indicate that miR-132 negatively modulates light-inducible expression of PER1 and PER2 in the SCN.

A deficit in a photic input pathway that couples light to the molecular clock, e.g. the ERK/MAPK cascade leading to CREB-dependent transcription (50), could account for the attenuation of both light-induced behavioral phase shifts as well as light-induced PER expression in the SCN of tTA::miR-132 mice. However, we found no difference in the levels of the phosphorylated, and active, forms of ERK1/2 and CREB in the SCN of tTA::miR-132 mice and non-transgenic controls following photic stimulation (data not shown and Supplementary Material, Fig. S6), thereby ruling out the possibility that the observed phenotypes in our mice are the result of an impairment in an input pathway that functions upstream of miR-132. Collectively, the data indicate that miR-132 transgenic expression in the SCN suppresses light-induced PER1 and PER2 expression via mechanisms that are downstream of ERK/MAPK and CREB activation.

The *Period* genes are transcriptionally regulated by MeCP2 via a CREB-dependent pathway

We next focused our attention on identifying *trans*-acting factors that may be involved in the transcriptional regulation

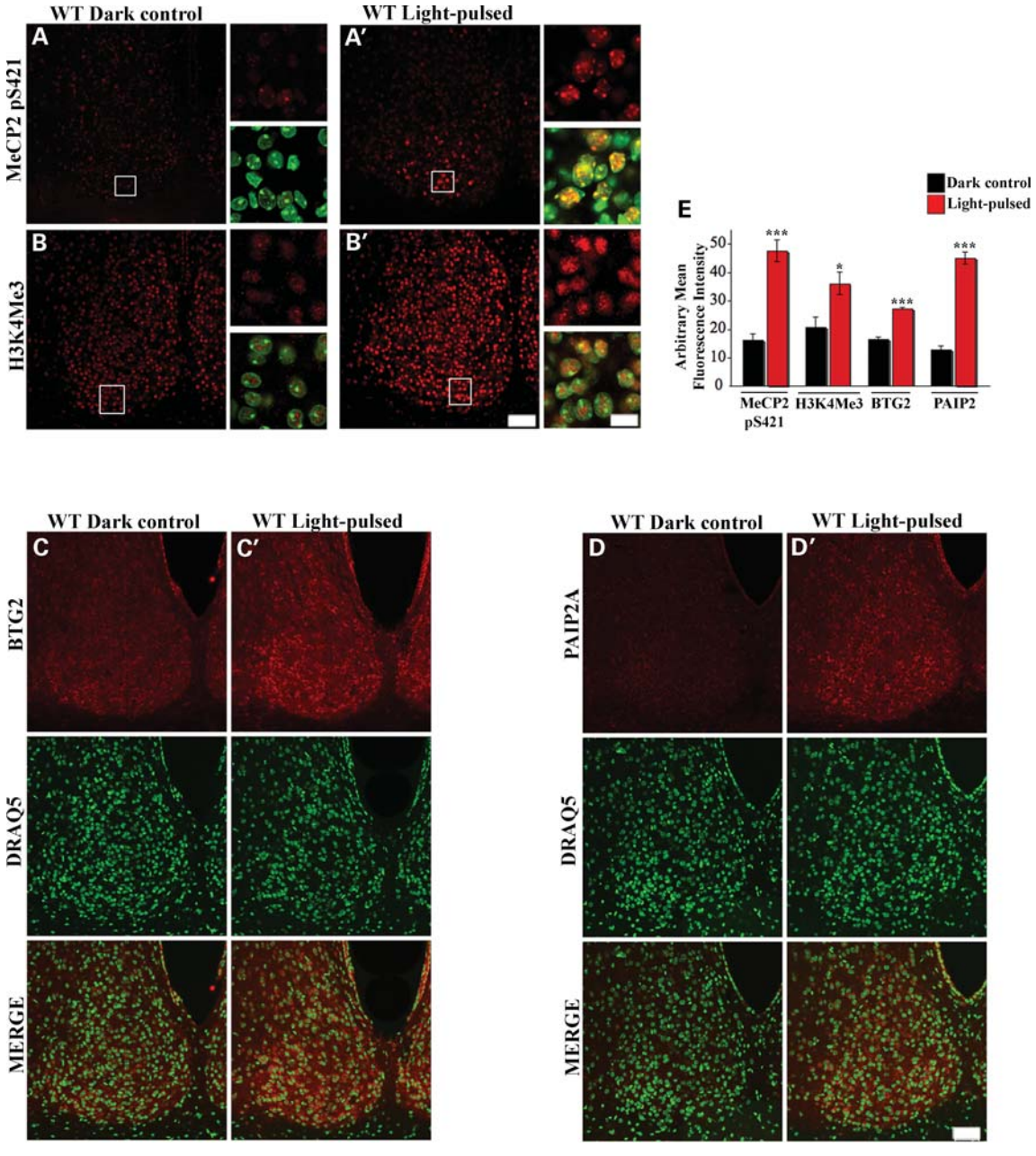

Figure 4. miR-132 targets and their downstream effectors are light-responsive. Light acutely induces the phosphorylation of MeCP2 at Ser421 (pS421) and trimethylation of histone H3 at lysine 4 (H3K4Me3) in the SCN. C57Bl/6 (WT) mice received a brief light pulse (15 min, 40 lux) at CT 15. Tissue was harvested 30 min after onset of light treatment and analyzed for expression of (**A'**) MeCP2 pS421 (red) or (**B'**) H3K4Me3 (red) by indirect immunofluorescence. Sections were counterstained with the nuclear marker, DRAQ5 (pseudocolored in green). (**A**, **B**) Dark control mice were not exposed to light but were killed at the same CT. For each condition, the boxed region in the left panel (scale bars = 50 μm) is presented in higher magnification in the right-most panels (scale bars = 5 μm): (top right) MeCP2 pS421 or H3K4Me3 immunoreactivity only; (bottom right) merged image of MeCP2 pS421 or H3K4Me3 immunoreactivity in combination with DRAQ5. BTG2 and PAIP2A protein levels in the SCN are induced in response to light. C57Bl/6 mice received a brief light pulse (15 min, 40 lux) at CT 15 and killed 2 h later for analysis of (**C'**) BTG2 (red) and (**D'**) PAIP2A expression (red) by indirect immunofluorescence. (**C**, **D**) Dark control mice were not exposed to light but were killed at the same CT. Scale bars = 50 μm. (**E**) Quantitation of light-induced expression of pS421 MeCP2, H3K4Me3, BTG2 and PAIP2A in the SCN. Values on the *y*-axis represent arbitrary mean fluorescence intensity for individual cells (in the case of pS421 MeCP2 and H3K4Me3) or for the unilateral SCN (in the case of BTG2 and PAIP2A). Values are presented as mean ± SEM. $n = 5$ mice per condition. $^{*}P < 0.05$, $^{***}P < 0.001$ versus dark control (two-tailed Student's *t*-test).

of the *Per1* and *Per2* genes. Several studies have already demonstrated that p300 positively regulates CLOCK-mediated transcription via histone H3 acetylation (6,51). Therefore, we chose to explore the role of MeCP2 in clock gene regulation, as it has been largely uncharacterized. MeCP2 has been classically viewed as a transcriptional repressor due to its affinity for methylated DNA (36,52). Nevertheless, recent evidence suggests that MeCP2-binding sites are located not only on CpG islands, but may also be found within intragenic regions (53). Moreover, it has been shown via genome-wide

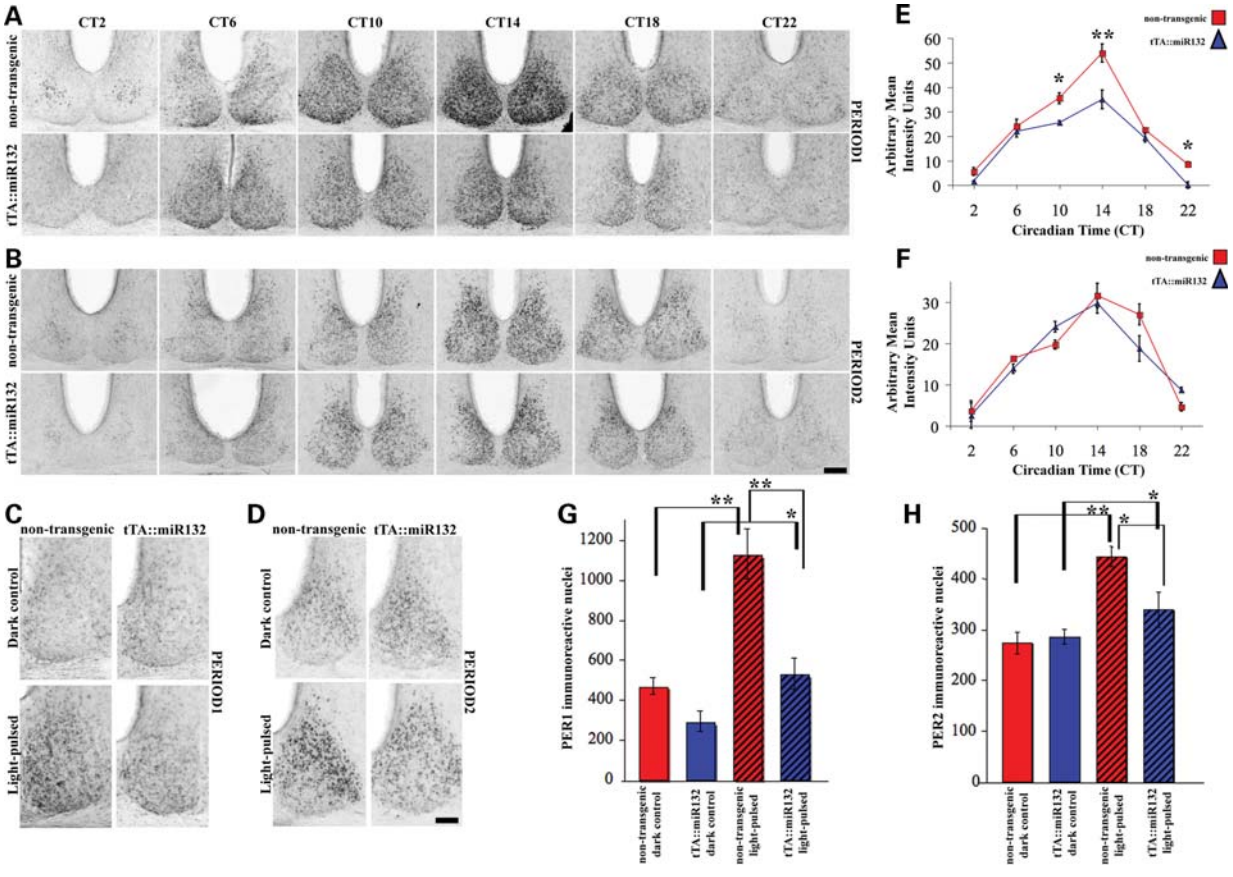

Figure 5. miR-132 overexpression in the SCN dampens PER1 protein rhythms and suppresses light-induced expression of PER1 and PER2. Rhythms of PER1, but not PER2, expression are dampened in the SCN of tTA::miR-132 mice. SCN tissue was harvested from tTA::miR-132 mice (bottom row) and non-transgenic controls (top row) at defined CT across a full circadian cycle, and analyzed for (**A**) PER1 and (**B**) PER2 expression by immunohistochemistry. Scale bars = 100 μm. Induction of PER1 and PER2 expression in the SCN in response to photic stimulation is attenuated in tTA::miR-132 mice. Non-transgenic and tTA::miR-132 mice received a brief light pulse (15 min, 40 lux) at CT 15 and SCN tissue was harvested 4 h later for determination of (**C**) PER1 and (**D**) PER2 levels by immunohistochemistry. Dark control mice were not exposed to light but were killed at the same CT. Scale bars = 50 μm. Quantitation of (**E**) PER1 and (**F**) PER2 rhythms from (A) and (B), respectively. Values on the *y*-axis represent the mean intensity of the unilateral SCN, given in arbitrary units. Quantitation of light-inducible (**G**) PER1 and (**H**) PER2 expression from (C) and (D), respectively. Values on the *y*-axis indicate the number of PER1- or PER2-immunoreactive nuclei in the bilateral SCN. Values are presented as mean ± SEM. $n = 4–6$ mice per group. $^{*}P < 0.05$, $^{**}P < 0.01$ (Fisher's LSD).

promoter analysis that a subset of MeCP2-bound promoters is actively expressed (30). These data suggest that MeCP2, besides acting as a transcriptional repressor, may also be involved in gene activation. Hence, we decided to examine whether MeCP2 binds to the *Per1* and/or *Per2* loci and whether it regulates their transcriptional activation and/or repression.

As a starting point to screen for putative MeCP2-binding sites in the *Per1* and *Per2* loci, we used the CpG plot algorithm (http://www.ebi.ac.uk/Tools/emboss/cpgplot/index.html) to identify putative CpG islands within 10 kb of the transcription start sites (TSSs). We identified two CpG islands in the *Per1* 5′-upstream region at bp −3333 to −3130 and at bp −3931 to −3536, herein referred to as *Per1* CpG islands #1 and #2, respectively (Fig. 6A). NIH-3T3 fibroblasts, a cell line that expresses *Per1* and *Per2* endogenously, were transiently transfected with the MeCP2-e1-myc isoform (54), and chromatin was harvested for ChIP experiments. We chose to use the MeCP2-e1 isoform, as it has been shown to be the predominant transcript in the murine hypothalamus (55), although the MeCP2-e2 isoform is also expressed. For these experiments, we observed typical transfection efficiencies within the range 15–25%. Via qPCR, we found enrichment of MeCP2 at CpG island #1 (4.5% relative to input, $P < 0.01$; Fig. 6C) and CpG island #2 (data not shown) of the *Per1* locus. We also identified a putative CpG island on the *Per2* locus at bp −481 to −57 (Fig. 6B). Conversely, we did not identify MeCP2 enrichment (<0.5% relative to the input) at this genomic location (Fig. 6D). Interestingly, we detected a very high enrichment of H3K4Me3 at CpG island #1 of *Per1* compared with the *Per2* CpG island (116% versus 9% relative to the input; Fig. 6C and D). Thus, the presence of MeCP2 in the *Per1* locus does not appear to interfere with the enrichment of H3K4Me3 in its vicinity, suggesting that the *Per1* gene is actively transcribed even in the presence of MeCP2.

In the second set of experiments, we chose to screen for MeCP2 enrichment at CRE (cAMP response element) sites and E-boxes of the *Per1* and *Per2* loci, known sites of light-inducible and circadian transcriptional regulation,

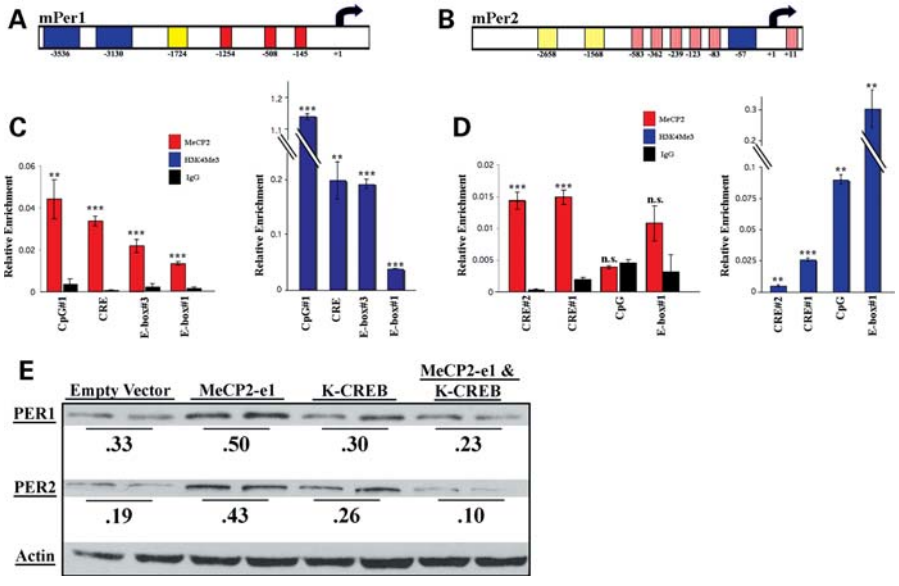

Figure 6. MeCP2 binds to elements within the mPer1 and mPer2 gene promoters and activates their transcription. Schematic representation of the (**A**) mPer1 and (**B**) mPer2 upstream regulatory elements. The mPer1 gene is composed of three canonical E-boxes (red box), one canonical CRE site (yellow box) and two CpG islands of ∼300 bp each (blue box). The mPer2 gene is composed of six non-canonical E-boxes (hatched red box), two non-canonical CRE sites (hatched yellow box) and one CpG island of ∼400 bp (blue box). Numbers below each box represent the genomic location relative to the TSS (+1; arrows). ChIP analysis for binding of MeCP2 (left) and H3K4Me3 (right) within the (**C**) mPer1 and (**D**) mPer2 promoters. Regions analyzed include (C) the CpG#1 (position −3130), CRE (position −1724), E-box#3 (position −1254) and E-box#1 (position −145) of the mPer1 gene, and (D) CRE#1 (position −1568), CRE#2 (position −2658), CpG (position −57) and E-box#1 (position +11) of the *mPer2* gene. ChIP assays were performed with chromatin harvested from NIH-3T3 cells 36 h following transient transfection with the MeCP2-e1-myc construct. Values on the *y*-axis indicate the enrichment of the immunoprecipitated (IP) DNA encompassing the specified region relative to an input control and are presented as mean ± SEM relative enrichment. Immunoprecipitation using an anti-rabbit IgG served as the negative control. Triplicate determinations from three independent experiments were made. $^{**}P < 0.01$, $^{***}P < 0.001$, n.s. = non-significant versus IgG (two-tailed Student's *t*-test). (**E**) Overexpression of the MeCP2-e1 isoform stimulates PER1 and PER2 expression in a CREB-dependent manner. Neuro-2a cells were transiently transfected with constructs encoding MeCP2-e1-myc (lanes 3 and 4), dominant-negative K-CREB (lanes 5 and 6) or both (lanes 7 and 8), and PER1 (top row) and PER2 (middle row) protein levels were examined 36 h later by western blotting. Transfection with empty vector pcDNA3 (lanes 1 and 2) served as the negative control. Actin expression served as the loading control. Values presented below each blot represent the mean relative abundance of the protein examined, normalized to actin expression, for each genotype. $n = 3$ per condition per experiment. The experiment was repeated three times and similar results were obtained.

respectively. We found MeCP2 enrichment (3% relative to the input, $P < 0.001$) at the *Per1* CRE site (Fig 6A and C). We also identified MeCP2 enrichment at the previously characterized E-box#3 and E-box#1 of the *Per1* locus (2.1 and 1.3%, respectively, relative to the input; Fig. 6A and C) (56). Similarly, we identified MeCP2 enrichment at both *Per2* CRE site #1 and *Per2* CRE site #2 (1.5% relative to the input, $P < 0.001$; Fig. 6B and D). It is noteworthy that MeCP2 and H3K4Me3 are co-enriched in the regions analyzed for the *Per1*, but not *Per2*, promoter. Also surprising is the lack of significant MeCP2 enrichment at the non-canonical E-box enhancer (E-box#1) found 11 nucleotides downstream of the *mPer2* TSS (Fig. 6B and D). A previous study indicated that this site accounts for much of the circadian transcriptional drive of the *mPer2* locus by CLOCK:BMAL1 (57). Moreover, all *Per2* E-boxes found upstream of E-box#1 also failed to show MeCP2 enrichment (data not shown), suggesting that MeCP2 is more highly enriched throughout the *Per1* domain in comparison.

In order to investigate whether MeCP2 activates or represses transcription of the *Period* genes and, if so, whether this regulation is mediated via a CREB-dependent mechanism, we immunoblotted for endogenous PER1 and PER2 in Neuro-2a cells that had been transiently transfected with constructs expressing MeCP2-e1 or dominant-negative CREB (K-CREB), or both (58). MeCP2-e1 overexpression alone induced ∼2-fold activation of PER1 and PER2, relative to empty vector control transfections (Fig. 6E). Importantly, MeCP2-dependent upregulation of PER1 and PER2 was completely abolished by co-transfection with K-CREB (Fig. 6E). The cumulative results indicate that MeCP2 binds to the *Per1* and *Per2* 5′ regulatory regions and that MeCP2 positively modulates transcription of the *Per1* and *Per2* genes via a CREB-dependent mechanism.

PAIP2A regulates the expression of PERIOD proteins in the murine SCN

The data thus far suggest that miR-132 negatively modulates light-induced clock resetting, in part, by downregulating the expression of certain chromatin remodeling factors (e.g. MeCP2, p300) that would otherwise participate in transcriptional activation of the *Period* genes. Nevertheless, the observed reduction in PER1 and PER2 protein levels in the SCN of tTA::miR-132 mice may also reflect the balance of other cellular processes that are perturbed in these mice, including regulation of protein translation.

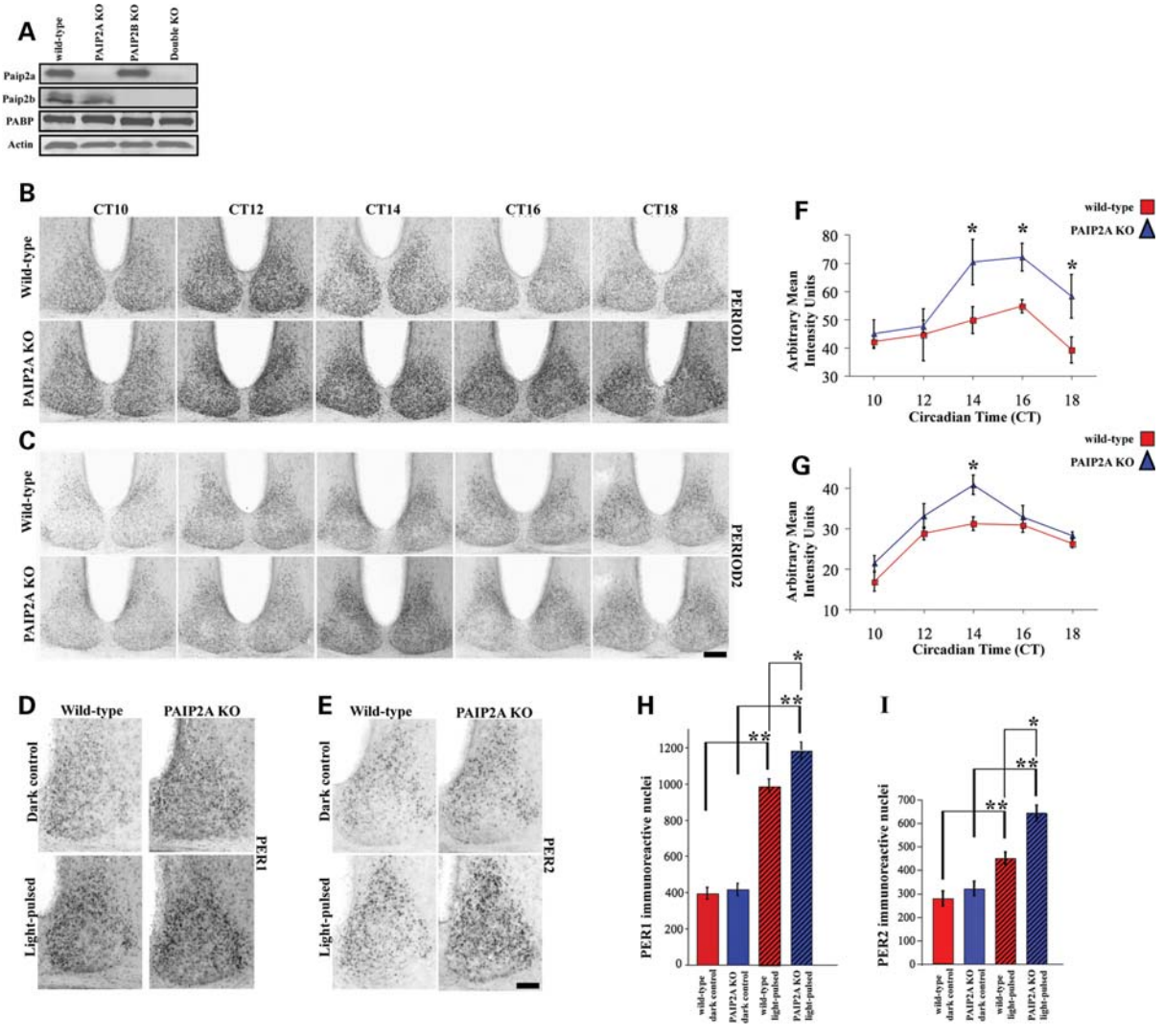

Figure 7. *Paip2a*$^{-/-}$ mice exhibit enhanced inducibility of PER1 and PER2 expression in the SCN in response to light and elevated basal expression of PER1 during the circadian night. (**A**) The absence of PAIP2A protein in the brains of *Paip2a*$^{-/-}$ mice. Brain extracts from wild-type (WT), *Paip2a*$^{-/-}$ (PAIP2A KO), *Paip2b*$^{-/-}$ (PAIP2B KO) and *Paip2a*$^{-/-}$*Paip2b*$^{-/-}$ (double knockout: DKO) mice were analyzed for PAIP2A, PAIP2B and poly(A)-binding protein (PABP) expression by western blotting. Expression of β-actin was used as a loading control. Expression of PER1 and PER2 in the SCN of wild-type and *Paip2a*$^{-/-}$ mice from the late subjective day to the mid-subjective night. SCN tissue was harvested from wild-type (top row) and *Paip2a*$^{-/-}$ mice (bottom row) at CT 10, 12, 14, 16 and 18, and analyzed for (**B**) PER1 and (**C**) PER2 expression by immunohistochemistry. Scale bars = 100 μm. Induction of PER1 and PER2 expression in the SCN in response to photic stimulation is potentiated in the absence of PAIP2A. Wild-type and *Paip2a*$^{-/-}$ mice received a brief light pulse (15 min, 40 lux) at CT 15 and SCN tissue was harvested 4 h later for determination of (**D**) PER1 and (**E**) PER2 levels by immunohistochemistry. Dark control mice were not exposed to light but were killed at the same CT. Scale bars = 50 μm. Quantitation of (**F**) PER1 and (**G**) PER2 protein abundance from (B) and (C), respectively. Values on the *y*-axis represent the mean intensity of the unilateral SCN, given in arbitrary units. Quantitation of light-inducible (**H**) PER1 and (**I**) PER2 expression from (D) and (E), respectively. Values on the *y*-axis indicate the number of PER1- or PER2-immunoreactive nuclei in the bilateral SCN. Values are presented as mean ± SEM. $n = 4–6$ mice per group. $^{*}P < 0.05$, $^{**}P < 0.01$ (Fisher's LSD).

We turned our attention to the potential role of PAIP2A in translational control of the PER proteins. The elevated expression of PAIP2A, a suppressor of eukaryotic translation, in the SCN of tTA::miR-132 mice may contribute to the down-regulation of PER1 and PER2 in these animals. To address this possibility, we examined the expression of PER1 and PER2 in the SCN of mice harboring a targeted deletion of PAIP2A (59). Western blot analysis confirmed the absence of PAIP2A protein expression in the brains of *Paip2a* knockout (*Paip2a*$^{-/-}$) mice (Fig. 7A). We first examined the effect of PAIP2A ablation on the basal expression of PER1 and PER2 within the SCN during an 8-h window of a circadian cycle, from the late subjective day (CT 10) to mid-subjective night (CT 18). This interval was chosen because it encompasses part of the rising phase as well as the declining phase of PER1 and PER2 protein rhythms; hence, mechanisms that either promote or inhibit translation of the cognate transcripts are likely to play a significant role during this time interval in determining the steady-state levels of PER proteins. The levels of PER1 expression in the SCN of wild-type littermates were moderate at CT 10, reached a peak at CT 12–14 and gradually declined thereafter (Fig. 7B). Notably, PER1 levels in the SCN were markedly elevated in *Paip2a*$^{-/-}$ mice at the later time points, when steady-state PER1 levels were falling in wild-

type controls (Fig. 7B and F). In contrast, we found no substantial difference in basal PER2 expression in the SCN of wild-type and *Paip2a*$^{-/-}$ mice at all time points examined, with the exception of CT14 (Fig. 7C and G). Importantly, the absence of PAIP2A did not significantly alter the CT 14 basal expression of two other proteins examined, MeCP2 and p300 (Fig. S7), arguing that PAIP2A is selectively regulating the basal expression of PER1 and is not globally affecting the SCN proteome. Moreover, it rules out the possibility that the downregulation of MeCP2 and p300 in the SCN of tTA::miR-132 mice is due to increased PAIP2A expression.

We further examined whether PAIP2A plays an essential role in regulating light-induced PER1 and PER2 expression in the SCN. We evaluated this hypothesis via administration of a brief light pulse (15 min, 40 lux) at CT 15 to *Paip2a*$^{-/-}$ and wild-type mice, and SCN tissue was harvested 4 h later to determine PER1 and PER2 expression. Light stimulation robustly increased the number of PER1-IR cells in the SCN of both wild-type and *Paip2a*$^{-/-}$ mice relative to their respective dark controls (Fig. 7D and H) but the number of PER1-IR nuclei in the SCN was significantly greater in light-pulsed *Paip2a*$^{-/-}$ mice compared with light-pulsed wild-type controls (Fig. 7H). Similarly, photic induction of PER2 expression in SCN cells was markedly potentiated in the absence of PAIP2A (Fig. 7E and I). These data indicate that PAIP2A plays a critical role in dampening light-induced expression of PER1 and PER2.

PAIP2A and BTG2 accelerate mRNA decay of *Period* transcripts

Numerous studies have shown that mRNA stability is regulated by deadenylation, or shortening of the poly(A) tail (60). PABP binds to and protects the poly(A) tail from deadenylation (61), whereas PAIP2A may have the opposite effect of promoting deadenylation (62). BTG2, as well, has been shown to stimulate mRNA decay by increasing the rate of deadenylation (39). Hence, the reduced levels of PER1 and PER2 proteins in the SCN of tTA::miR-132 mice may, in part, be due to changes in mRNA decay kinetics arising from altered PAIP2A and BTG2 expression. We tested whether or not the turnover rates of Per1 and Per2 mRNAs are affected by PAIP2A and BTG2 using two experimental paradigms.

In the first approach, we generated reporter constructs carrying full-length Per1 and Per2 under the control of a Tet-responsive promoter. Reporters were transfected in HEK293-TOF cells, which stably express the Tet-OFF transcriptional activator, together with a plasmid that constitutively expresses PAIP2A or BTG2. Twenty-four hours post-transfection, transcriptional chase experiments were performed by adding doxycycline (2 μg/ml) in the culture medium to block further transcription of the reporter. Quantitative RT-PCR analyses revealed that the turnover rate of both Per1 and Per2 reporters was accelerated by the overexpression of PAIP2A or BTG2, compared with control cells that had been transfected with pcDNA3 empty vector (Fig. 8A and B).

In the second approach, we assessed the stability of endogenous Per1 and Per2 mRNA in Neuro-2a cells that inducibly express PAIP2A or BTG2. Neuro-2a cells were transfected with expression constructs encoding PAIP2A or BTG2 under the control of a Tet-responsive promoter, together with the Tet-OFF transcriptional activator. Immediately after transfection, cells were maintained in a culture medium containing doxycycline (200 ng/ml) for 24 h, at which point they were transferred to medium lacking doxycycline for an additional 9 h to induce PAIP2A or BTG2 expression. Subsequently, actinomycin D (5 μg/ml) was added to inhibit *de novo* RNA synthesis, allowing us to analyze the turnover of pre-existing pools of endogenous Per1 and Per2 mRNA. Similar to the reporter experiments, quantitative RT-PCR analyses showed that overexpression of either PAIP2A or BTG2 increased the rate of decay of endogenous Per1 and Per2 mRNA, relative to control cells that had been transfected with an empty vector (Fig. 8C and D).

The cumulative data indicate that PAIP2A and BTG2 overexpression promotes the decay of Per1 and Per2 mRNA. On the basis of these results, we propose that by regulating the expression of its targets—PAIP2A and BTG2—miR-132 indirectly alters the stability of Per1 and Per2 transcripts and, consequently, translation of PER proteins.

DISCUSSION

In this report, we have shown that miR-132 likely regulates a number of target genes that are associated with chromatin remodeling (MeCP2, p300, JARID1A) and protein translation (BTG2, PAIP2A) (Fig. 1). Overexpression of miR-132 in the SCN in a transgenic mouse model attenuates phase shifts of wheel-running behavior in response to nocturnal light pulses (Fig. 2). Upregulated miR-132 expression in the transgenic SCN is accompanied by an anticipated reduction in the expression of MeCP2, p300, JARID1A and BTG2 in the SCN, but an unexpected increase in the other predicted target, PAIP2A (Fig. 3). Further evidence supporting the authenticity of these five miR-132 targets comes from miR-132 knockdown experiments *in vitro* in Neuro-2A cells (Fig. 1) and *in vivo* in the SCN of intact mice (Fig. 3). Moreover, similar to miR-132 itself [which is a light-inducible microRNA (19)], the expression or activity of its targets also appears to be regulated by light (Fig. 4). miR-132 overexpression in the SCN dampens PER1 rhythms as well as photic activation of PER1 and PER2 expression (Fig. 5). Additional data reported here provide a link between three miR-132 targets (namely MeCP2, PAIP2A and BTG2) and *Per1* and *Per2*. First, results from our chromatin immunoprecipitation (ChIP) analysis and MeCP2 overexpression experiments suggest that MeCP2 binds to the promoters of the *Per1* and *Per2* genes and activates their transcription (Fig. 6). Second, using *Paip2a* knockout mice, we show that PAIP2A dampens light-induced expression of PER1 and PER2, as well as basal expression of PER1, in the SCN (Fig. 7). Third, expression of PAIP2A or BTG2 accelerates the decay of *Per1* and *Per2* transcripts (Fig. 8). Collectively, our observations suggest that miR-132 negatively regulates light-induced entrainment of the circadian clock by modulating the expression of a set of target genes that influences chromatin remodeling as well as protein translation and that ultimately impinges upon PER expression in the SCN (Fig. 9). The evidence further suggests that light triggers waves of molecular events that initially

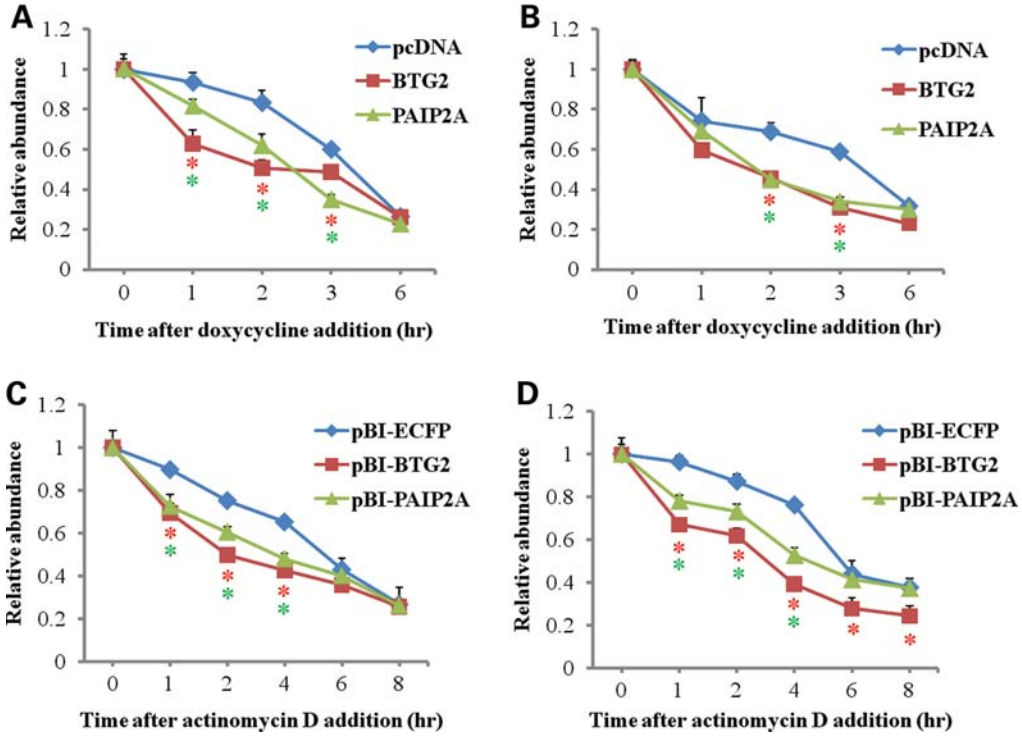

Figure 8. PAIP2A and BTG2 overexpression increases the turnover of Per1 and Per2 transcripts. Transcriptional chase experiments showing levels of (**A**) Per1 and (**B**) Per2 reporters in the presence of ectopically expressed PAIP2A or BTG2. HEK293-TOF cells were transfected with either pBI-Per1 or pBI-Per2 reporter plasmids, together with PAIP2A- or BTG2-expressing constructs or empty plasmid (pcDNA). Levels of (**A**) Per1 and (**B**) Per2 reporter transcripts were determined by qRT-PCR at indicated times (*x*-axis: in hr) after addition of doxycycline (2 μg/ml). Values on the *y*-axis indicate normalized relative abundance, where, for each transfection condition, the level of reporter expression at time = 0 h was set arbitrarily at 1. Values are normalized to 18S rRNA expression. Levels of endogenous (**C**) Per1 and (**D**) Per2 transcripts following induction of PAIP2A or BTG2 expression. Neuro-2a cells were transfected with tet-inducible PAIP2A (pBI-PAIP2A) or BTG2 (pBI-BTG2) expression plasmids, or an empty plasmid (pBI-ECFP), together with the Tet-OFF transcriptional activator. Cells were maintained for 24 h in medium containing doxycycline (200 ng/ml), and then transferred to Dox-free medium for an additional 9 h to induce PAIP2A or BTG2 expression. Actinomycin D (5 μg/ml) was subsequently added to the culture medium. Levels of (**C**) Per1 and (**D**) Per2 transcripts were determined by qRT-PCR at indicated times (*x*-axis: in hr) after addition of actinomycin D. Values on the *y*-axis indicate normalized relative abundance, where, for each transfection condition, the level of Per1/Per2 expression at time = 0 h was set arbitrarily at 1. Values are normalized to 18S rRNA expression. Error bars represent the standard deviation from triplicate determinations of a single representative experiment. Consistent results were obtained from three independent experiments. $^{*}P < 0.05$ versus empty vector control (Fisher's LSD).

facilitate the resetting response, but also sets in motion events (e.g. induction of miR-132) that, later on, act in a feedback inhibitory fashion to dampen the response and restore the SCN to homeostasis (Fig. 9). This report also raises the tantalizing possibility that miRNAs, in general, and miR-132, in particular, effect the biological outcome, not necessarily through their repressive action on a single target, but through coordinated regulation of multiple targets that play a role in a shared biological process.

Our previous work (19) implicated miR-132 as a negative modulator of light-induced clock entrainment but did not identify a bona fide target of miR-132 within the SCN, thus leaving unanswered the molecular mechanisms governing the behavioral phenomenon. Through our interrogations of various computational target prediction algorithms, we noted a considerable number of predicted targets with the common functions of regulating chromatin architecture and hence gene transcription, or regulating mRNA stability and protein translation. We confirmed this abundance by systematically comparing the percentage of target genes in these functional categories across all vertebrate microRNAs. This observation led us to the proposition that genes which participate in a common biological process or pathway, or which functionally interact, are co-regulated by an overlapping set of miRNAs. Recent work indicating that the core pluripotency factors, OCT4, SOX2 and KLF4, which determine stem cell fate, are all under the regulation of a single miRNA, miR-145, supports this notion (26). One may speculate that, depending on differences in the spatiotemporal expression of a set of miRNAs, their common targets may be regulated by only one of these miRNAs in a given cellular context, or co-regulated in the same cell at a specific time by multiple miRNAs that work in unison to modulate a cell-specific physiological process.

Using our tTA::miR-132 mice, we identified a number of predicted targets whose expression in the SCN is repressed by miR-132: MeCP2, p300, JARID1A and BTG2. For these factors, the target sites (MREs) that are identified by the various computational target prediction algorithms directly mediate the repressive effects of miR-132. However, in the case of PAIP2A, despite the fact that 3′UTR luciferase assays confirmed the functionality of the predicted target site, and *in vitro* as well as *in vivo* knockdown of miR-132 evoked an increase in endogenous PAIP2A expression, PAIP2A levels in the transgenic SCN were unexpectedly

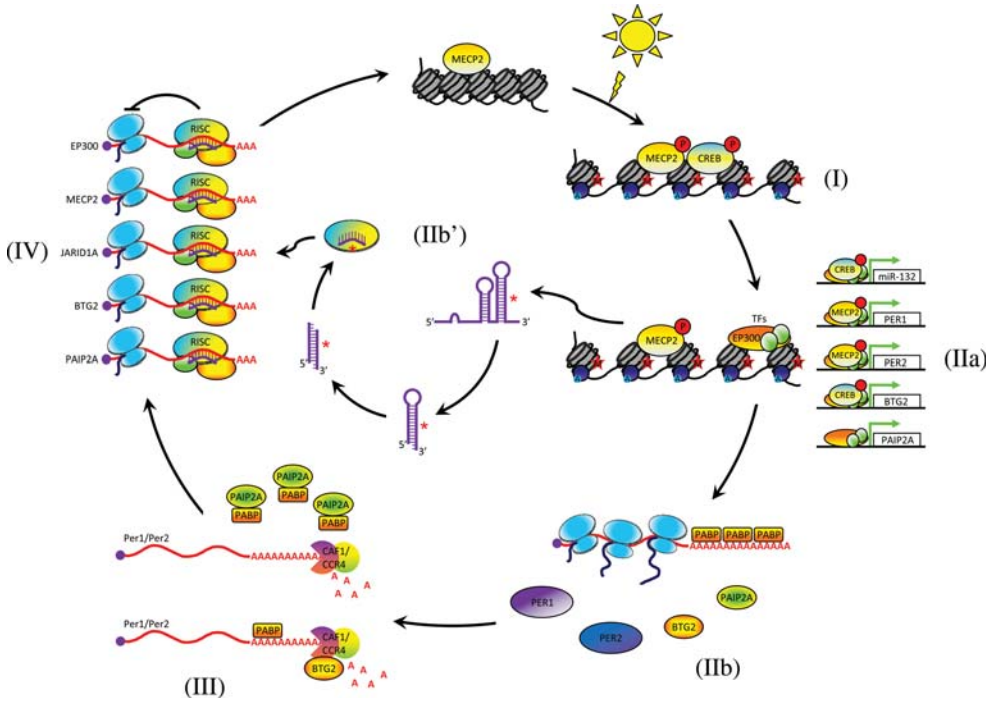

Figure 9. Proposed model of light-induced molecular waves of clock entrainment. (**I**) Nocturnal light exposure triggers rapid, post-translational events in SCN neurons that promote remodeling of chromatin to a transcriptionally permissive state. For instance, a brief light pulse elicits the phosphorylation (P) of MeCP2 at Ser421, trimethylation (M) of histone H3 at lysine 4 (red star) and acetylation (A) of histone H2A.Z at lysine residues K4, K7 and K11 (purple circle). (**IIa**) As a result, transcription factors (TFs) and their co-modulators (e.g. MeCP2 and EP300) gain access to gene promoters and transactivate a number of light-responsive genes, including *Per1*, *Per2*, *Btg2* (29), miR-132 (19) and possibly *Paip2a*. (**IIb**) Subsequent mRNA translation leads to increased protein abundance of PER1, PER2, BTG2 and PAIP2A. PABP physically associates with the polyA tails of the transcripts and facilitates translation. (**IIb'**) Meanwhile, the primary miR-132 transcript undergoes a series of processing steps, including sequential proteolytic cleavages to generate the pre-miR-132 stem loop and the miRNA duplex, export of pre-miR-132 to the cytoplasm and incorporation of the mature strand (denoted by the red asterisk) into the RNA-induced silencing complex (RISC). (**III**) As the levels of BTG2 and PAIP2A proteins increase, further translation of *Per1* and *Per2* transcripts is inhibited. PAIP2A competes with the polyA tail for binding to PABP, thus inhibiting PABP-dependent facilitation of translation; moreover, PAIP2A may promote transcript degradation (62). BTG2 can physically associate with the CAF1/CCR4 deadenylase complex and enhances CAF1/CCR4-mediated deadenylation and mRNA decay (39). (**IV**) With rising levels of mature miR-132, miRNA-mediated translational repression of miR-132 targets (ep300, mecp2, jarid1a, btg2, paip2a) ensues, restoring homeostasis to those processes that were triggered by light.

upregulated. The collective data suggest to us that PAIP2A is an authentic miR-132 target. Nevertheless, as demonstrated in this report, miR-132 upregulation in the SCN perturbs the expression of multiple targets and, by extension, the genetic networks in which these targets are embedded. The steady-state levels of PAIP2A (as with any protein) reflect the balance of transcription, translation, mRNA decay and protein turnover, and it is therefore conceivable that network perturbations affecting any of the aforementioned processes could mask the direct effects of miR-132 on PAIP2A expression. The mechanisms that underlie the increase in PAIP2A expression in tTA::miR-132 mice are unknown and beyond the scope of this current study. Preliminary evidence rules out an involvement of MeCP2- and p300-dependent transcriptional mechanisms, because overexpression of neither factor in Neuro-2a cells discernibly affects the expression of PAIP2A (data not shown). It remains to be determined whether the elevated levels of PAIP2A in the transgenic SCN are linked to the increase in the H3K4Me3 mark or the decrease in BTG2 (which, as an inducer of mRNA deadenylation, would be predicted to prolong the half-life of mRNAs upon its downregulation), or to a hitherto unexplored mechanism.

One of the key advances of this study is the establishment of a mechanistic link between MeCP2 and *mPer1* and *mPer2* expression. A previous study reported that pS421 MeCP2 expression is induced in the SCN following photic stimulation (28), but did not further examine the consequences of this phosphorylation or MeCP2 expression as they pertain to the cellular physiology of circadian oscillators. From our current work, we conclude the following: (1) MeCP2 promotes or permits the expression of *mPer1* and *mPer2*; (2) MeCP2-dependent transactivation of *mPer1* and *mPer2* expression is mediated via a CREB-dependent pathway; and (3) MeCP2 interacts physically with 5′ regulatory elements of the *mPer1* and *mPer2* genes. Regarding points (1) and (2), it is interesting to note that although MeCP2 was originally characterized as a transcriptional repressor, a recent report profiling hypothalamic gene expression in *Mecp2*-null as well as *Mecp2*-overexpressing mice revealed that MeCP2 activates, rather than represses, the majority (∼85%) of the genes that displayed altered expression (30). Even more fascinating was their observation that, in the case of MeCP2-activated genes, MeCP2 physically and functionally cooperates with CREB at promoter sites to actuate gene transcription (30). This functional interplay between MeCP2 and CREB is of potential

relevance in the case of light-triggered transcriptional activation within the SCN, which requires the actions of CREB (63). It would be tempting to further propose that light-induced phosphorylation of MeCP2 facilitates the functional dynamic between MeCP2 and CREB, thereby enhancing CREB-dependent transcription in the SCN.

By demonstrating that MeCP2 is physically bound to the promoters of *mPer1* and *mPer2*, our ChIP analysis establishes, for the first time, a direct link between MeCP2 and the *Per* genes. In particular, MeCP2 is enriched at all 5′ regulatory elements within 10 kb of the *mPer1* TSS that were examined: this encompasses a CpG island, a CRE site and previously characterized E-boxes proximal to the TSS. This is in stark contrast to the distribution of MeCP2 within the *mPer2* promoter: MeCP2 enrichment was restricted to the two CRE sites examined and was not detected within a region proximal to the TSS that encompasses a CpG island and the functional E-box enhancer (57). These data raise the tantalizing possibility that MeCP2 differentially regulates *mPer1* and *mPer2* transcription. Notably, miR-132 upregulation in the SCN elicits differential effects on PER1 and PER2 expression: although light-inducible expression is attenuated for both proteins in our transgenics, only PER1 exhibits a dampening of rhythmic expression. This suggests that one (or more) of the targets of miR-132 is (are) responsible for the divergent effects on *mPer1* and *mPer2* expression. Previous work by our group and others has hinted at the possibility that *mPer1* and *mPer2* expression are regulated by overlapping but distinct mechanisms (48,64). It is not inconceivable that the dampening of PER1 rhythms in the tTA::miR-132 transgenics may be due, in part, to a reduction in a potential facilitatory effect of MeCP2 on E-box-mediated transcription of the *mPer1* gene, but not of the *mPer2* gene. It would also be interesting to explore the possibility of a functional interaction between MeCP2 and p300, which has been shown to augment CLOCK/BMAL1-mediated transcription (6), at the *mPer1* E-boxes. Lastly, although H3K4Me3 expression was enhanced in the SCN of our transgenics (arguably due to suppressed JARID1A expression), we did not observe a global increase in gene expression. This is consistent with the notion that the H3K4Me3 mark places chromatin in a transcriptionally permissive state, but other factors are required in order to fully activate a particular gene.

A seminal discovery arising from this work is the involvement of PAIP2A in translational control of core clock mechanisms. Extensive and elegant biochemical analyses have established PAIP2A as a potent translational inhibitor via displacement of PABP from the poly(A) tail, thereby abrogating PABP-dependent enhancement of EIF4G-mediated translation. Here, we characterized the function of PAIP2A in the translational control of the PERIOD proteins. Our work shows that PAIP2A is an essential negative modulator of light-induced PER1 and PER2 expression, because genetic deletion of *Paip2a* potentiates the expression of both proteins in response to photic stimulation. Significantly, the inverse phenotypes between the *Paip2a*-null and the tTA::miR-132 mice with respect to PER protein expression suggest that PAIP2A upregulation in our miR-132 transgenics contributes, in part, to the attenuated induction of PER1 and PER2 in response to light. Furthermore, we noted that, in the absence of PAIP2A, basal expression of PER1 during the first half of the circadian night is elevated. The effect of *Paip2a* abrogation on basal PER2 expression is more subtle by comparison. Notably, these results correlate with those obtained in the tTA::miR-132 transgenics, in which PER1 rhythms are dampened without a discernible effect on PER2 rhythms. Our *in vivo* data point to the differential regulation of PER1 and PER2 translation control via PAIP2A under certain physiological conditions. Lastly, the fact that miR-132 co-regulates the expression of both PAIP2A and BTG2, a factor that promotes poly(A) deadenylation and thus inhibits translation, raises the intriguing possibility that there are multiple checkpoints that control and fine-tune the level of translation in our transgenics. Indeed, our *in vitro* studies suggest that PAIP2A- and BTG2-regulated mRNA decay may play a role in setting the levels of PER1 and PER2 protein expression in the SCN.

The current study provides a novel paradigm in miR-132-dependent regulation of circadian clock entrainment, in which miR-132 fine-tunes the expression of gene clusters involved in chromatin remodeling and translation control. Our data lead us to propose a model for clock entrainment, in which light induces a temporal series of key molecular events—from rapid post-translational modifications to slower events such as gene transcription—that are required for the acute changes in gene expression which accompany photic resetting (Fig. 9). Light-induced miR-132 expression leads to the ultimate stage of this ‘molecular wave’, whereby the processes that were first triggered by photic stimulation are eventually restored to homeostasis (Fig. 9). Furthermore, we propose that this ability of one miRNA to coordinate the expression of functionally related genes is not confined to miR-132, but rather that miRNAs, in general, have evolved to orchestrate and tightly regulate cell-specific physiological processes via their actions on these related genes. In conclusion, our results leave open the possibility for future studies that address the role of aberrant expression of miR-132 and its downstream targets as a contributing factor in the various human pathophysiological conditions that are linked to disturbances in circadian rhythms.

MATERIALS AND METHODS

A more detailed description of Materials and methods is available in the Supplementary Material.

Generation of pBI-miR-132-ECFP transgenic mice and animal husbandry

DNA of the pBI-miR-132-ECFP construct was linearized, purified and injected into the pronuclei of oocytes from FVB/N mice at the Ohio State University Transgenic Facility. Founders were identified by PCR genotyping using the following primers: (fwd) 5′-GGAAGGAGAGCAAACACAGC-3′ and (rev) 5′-CGTCTAGACTACACATTGATCCTAGCAGAAG-3′. Founders were backcrossed for a minimum of four generations onto a C57BL/6J background prior to analysis. All animal handling and experimental procedures were approved by the Animal Welfare Committee of the University of Ottawa in accordance with the institutional guidelines.

Computational analyses on the functional annotations of microRNA-predicted targets

miRNA targets were obtained from TargetScan (release 5.1 April 2009). We restricted the analysis to the set of miRNAs belonging to the same family as miR-132, i.e. conserved across most vertebrates. We then focused on miRNAs with 50 or more predicted conserved targets. We used the GO annotations from the MGI database. For each microRNA, we measured the frequency of its conserved targets that are annotated with GO terms 'chromatin modification' (GO:0016568) and/or 'chromatin assembly or disassembly' (GO:0006333) and GO term 'translation' (GO: 0006412) and/or any of their children terms in the ontology.

Vector construction

The full-length 3′-UTRs of *Btg2*, *Paip2a*, *Ep300* and *Jarid1a* were amplified by PCR from bacterial artificial chromosome (BAC) constructs. Primer sequences are provided in the Supplementary Material. The 3′-UTRs were cloned into the pGL3-Control vector (Promega, Madison, WI, USA), between the luciferase (*luc*+) gene and the SV40 late poly(A) signal. For the *Mecp2* gene, a 9.5 kb *Ale*I–*Xma*I fragment encompassing the entire 3′-UTR was excised from a BAC construct (Clone ID number RP23-396E2; BACPAC Resources Center, Oakland, CA, USA) and inserted between the *luc*+ gene and the SV40 poly(A) signal of the pGL3-Control vector. Full-length cDNAs of mPer1, mPer2, Btg2 and Paip2A were cloned into the pBI-ECFP Tet vector to generate pBI-Per1, pBI-Per2, pBI-BTG2 and pBI-PAIP2A vectors, respectively, all of which co-express ECFP in a Tet-inducible manner. Site-directed mutagenesis of the predicted MREs of the various 3′UTRs was performed using the QuikChange® Site-Directed Mutagenesis Kit (Stratagene, Santa Clara, CA, USA).

Cannulation and infusion

Lateral ventricle cannulations and drug infusions were performed as described previously (65). Infusion of antagomirs (Dharmacon, Lafayette, CO, USA; 100 μM, 3 μl in saline) was performed at the indicated CT.

Behavioral and photic stimulation paradigms

Mice were individually housed in polycarbonate cages equipped with a running wheel in ventilated cabinets with timer-controlled lighting (white LED lighting ∼100 lux at the cage level). To monitor wheel-running activity, cages were equipped with magnetic switches, and switch closures were recorded with the ClockLab® software (Coulbourn Instruments, Whitehall, PA, USA). Beginning at 6–8 weeks of age, adult male mice were singly housed in the wheel-running cages and stably entrained to a 12 h:12 h light:dark (LD) cycle for at least 14 days prior to release into constant darkness (DD). After 12–14 days in DD, mice received a brief light pulse of medium light intensity (40 lux) for 15 min at CT 15 and returned to DD for an additional 12–14 days. Subsequently, mice received a second light pulse of high light intensity (400 lux) for 15 min at CT 15, and afterwards returned to DD for 12–14 days. For the doxycycline reversal experiments, mice were fed *ad libitum* rodent chow containing doxycycline (6 mg/g food; Bio-Serv, Frenchtown, NJ, USA) for 4 weeks while being maintained, singly housed in wheel-running cages, in a fixed 12 h:12 h LD cycle. After ∼3 weeks of Dox feeding, mice were released into DD conditions, and 5–7 days thereafter, mice received a single light pulse (40 lux, 15 min) at CT 15. Measurements of light-induced phase shifts and period length were performed as described previously (19).

Immunofluorescent/immunohistochemical detection and western blotting

Immunofluorescent labeling, immunohistochemistry (IHC) and western blotting were conducted as described previously (65). Antibody dilutions are provided in the Supplementary Material.

Cell culture and transfection

Neuro-2a (ATCC, American Type Culture Collection, Manassas, VA, USA) and HEK293-TOF (Clontech) cells were grown on 6-well plates and transfected using Lipofectamine 2000 (Invitrogen, Carlsbad, CA, USA) according to the manufacturer's instructions. Detailed descriptions of each transfection, including the quantities of each vector or microRNA hairpin inhibitor, are provided in the Supplementary Material. To examine the effects of BTG2 or PAIP2A expression on the turnover of a Per1 or Per2 reporter, HEK293-TOF cells (Clontech) were transfected with 1 μg of pBI-Per1 or pBI-Per2 reporter constructs together with 3 μg of pAC-BTG2 or pCMV-SPORT6-PAIP2A expression constructs and 0.2 μg of pCS-Venus vector. Twenty-four hours post-transfection, cells were transferred to a culture medium containing doxycycline (2 μg/ml; Sigma-Aldrich), and RNA was harvested at indicated times post-Dox treatment. To examine the effects of BTG2 or PAIP2A expression on the turnover of endogenous mPer1 or mPer2 transcripts, Neuro-2a cells were grown on 6-well plates and transfected with 1 μg of pBI-BTG2 or pBI-PAIP2A expression vectors together with 3 μg of pTet-OFF expression vector and 0.2 μg of pCS-Venus vector (Clontech). Following transfection cells were maintained on the culture medium supplemented with doxycycline (200 ng/ml) for 24 h, and then transferred to Dox-free medium for an additional 9 h to induce BTG2 or PAIP2A expression. Subsequently, cells were treated with the medium containing actinomycin D (5 μg/ml; Sigma-Aldrich), and RNA was harvested at indicated times following actinomycin D addition.

Luciferase assays

HEK293 and Neuro-2a cells were grown on 24-well plates and transfected with 12.5 ng of pRL-TK (Promega), 200 ng of pGL3 constructs containing the 3′UTRs of the respective genes, and 25 pmol of miRIDIAN® mmu-miR-132 Mimic or miRIDIAN® microRNA Mimic negative control #1 (Dharmacon) using Lipofectamine 2000. Cell lysates were prepared 24 h post-transfection and processed using the Dual Glo® Luciferase Assay System (Promega).

Chromatin immunoprecipitation

NIH-3T3 cells ($\sim 2 \times 10^7$) were transiently transfected with 48 μg of pcDNA3.1-hMeCP2-e1-myc, along with 6 μg of pCS-Venus to monitor transfection efficiency. Thirty-six hours post-transfection, cells were cross-linked with 1% formaldehyde for 15 min at room temperature (RT) and quenched for 5 min at RT with 125 mM glycine. Cell pellets were then resuspended in 50 mM HEPES–KOH, pH 7.5, 140 mM NaCl, 1 mM EDTA, 1% Triton-X-100, 0.1% sodium deoxycholate, 0.1% SDS and protease inhibitor cocktail, and sonicated for 80 cycles to an average size of ~800 bp using a 4°C sonicator (Bioruptor® UCD-200, Diagenode, Inc., Sparta, NJ, USA). Immunoprecipitation was performed overnight at 4°C with 5 μg of mouse anti-myc (Sigma-Aldrich), 5 μg of rabbit anti-MeCP2 (Abcam), 3 μg of rabbit anti-H3 (Abcam), 5 μg of rabbit anti-H3K4Me3 (Millipore) and 5 μg of anti-rabbit IgG (Jackson Immunoresearch, West Grove, PA, USA). Immune complexes were captured with 100 μl of 50% GammaBind Plus Sepharose Beads (GE Healthcare, Piscataway, NJ, USA) for 2 h at 4°C. DNA complexes were eluted from the beads with 150 μl of 1% SDS, 0.1 M $NaHCO_3$, pH 8.0, and heated at 55°C overnight with 100 μg of proteinase K (Invitrogen). DNA fragments were phenol:chloroform extracted and resuspended in 100 μl of TE, pH 8.0. Two microliters of DNA were used per reaction for qPCR analysis.

Reverse transcription

SCN tissue was pooled from three mice of the same genotype, and total RNA was isolated using the *mir*Vana™ miRNA Isolation Kit (Applied Biosystems, Foster City, CA, USA). Total RNA (10 ng) was reverse transcribed using the TaqMan® MicroRNA Reverse Transcription Kit (Applied Biosystems) and miR-132- or miR-219-specific stem-loop primers. To determine the abundance of Per1 and Per2 transcripts, RNA was harvested from HEK293-TOF or Neuro-2a cells using the TRIzol® reagent (Invitrogen) according to the manufacturer's instructions, and reverse transcribed using Superscript™ III Reverse Transcriptase (Invitrogen).

Quantitative real-time PCR

Real-time PCR for mature miR-132 and miR-219 was performed using TaqMan® microRNA assay (Applied Biosystems) on the Rotor-Gene 6000 Real-Time Rotary Analyzer (Corbett Life Science, Concorde, New Zealand). For qPCR analysis of ChIP DNA and cDNA, PCRs were carried out using the ABsolute™ Blue QPCR SYBR® Green Mix (ABgene, Ltd., Rockford, IL, USA) and run under the following conditions: one cycle at 95°C for 15 min, and 50 cycles at 95°C for 15 s, 60°C for 30 s and 72°C for 30 s. The sequences of qPCR primers are provided in the Supplementary Material.

Image acquisition

Immunohistochemistry images were acquired using a 20× objective with a Zeiss Axiovert Observer Z1 epifluorescent/light microscope equipped with an AxioCam MRm cooled-color camera (Oberkochen, Germany). Immunofluorescent tissue sections were examined and images were captured using a Zeiss 510 laser scanning confocal microscope with argon (488 nm), helium/neon (546 nm) and helium/neon (633 nm) lasers. For mPer1 and mPer2 rhythms and immunofluorescent light inductions, central SCN images were inverted and the SCN was outlined using a polygon. The '*measure*' function in ImageJ (http://rsbweb.nih.gov/ij) yielded a 'mean gray' value for the SCN. Background values were obtained from non-immunoreactive tissues in the lateral hypothalamus. For mPer1 and mPer2 light induction experiments, images were assigned a minimal threshold using a grayscale threshold value between 0–100 and 0–120. For IHC light inductions, a polygon was used to outline the SCN, and the '*analyze particles*' tool yielded a count of particles along with each corresponding particle area. We excluded particles with less than 50 pixels per area, and subsequent summation yielded total area of immunoreactive SCN cells. This area divided by an average cell size of 120 pixels produced an estimated cell count per unilateral SCN.

SUPPLEMENTARY MATERIAL

Supplementary Material is available at *HMG* online.

ACKNOWLEDGEMENTS

We thank the following individuals for the generous gift of reagents: J. Zhou (anti-pS421 MeCP2 antibody), S. Tajima (anti-DNMT3A antibodies), D. Weaver (anti-mPER2 antibodies), S. Reppert (anti-mPER1 antibody), L. Berthiaume (anti-GFP antibodies), S. Impey (pCAG-miR-132 vector), A. Nagy (pCX-ECFP vector), A. Miyawaki (pCS-Venus vector), B. Minassian (hMeCP2-e1-myc vector), J. Wu (pAC-BTG2 vector) and H. Okamura (pcDNA3-mPER1 and pBS-mPER2 vectors). miR-132 transgenic mice were generated by H.-Y.M.C. in the laboratory of K. Obrietan at the Ohio State University. The authors wish to thank K. Obrietan for generously allowing the use of these mice for the present study. M.A.-S. designed, performed and analyzed the experiments. G.A. and R.O.-H. provided technical help. D.C.-P. assisted in quantification and statistical analyses. C.P.-I. designed and performed computational analyses. A.Y. and N.S. provided Paip2A knockout mice. H.-Y.M.C. conceived the study, designed, performed and analyzed the experiments, and wrote the manuscript. The authors wish to dedicate this work to Lucas Cheng.

Conflict of Interest statement. None declared.

FUNDING

This work was supported by an operating grant from the Canadian Institute of Health Research (CIHR) #086549 (to H.-Y.M.C.) and an infrastructure grant from the Canadian Foundation for Innovation (CFI). H.-Y.M.C. is a Canada Research Chair (CRC) Tier II in the Genetics of Biological Timing and a recipient of the Early Researcher Award from the Ontario Ministry of Research and Innovation.

REFERENCES

1. Reppert, S.M. and Weaver, D.R. (2002) Coordination of circadian timing in mammals. *Nature*, **418**, 935–941.
2. Toh, K.L., Jones, C.R., He, Y., Eide, E.J., Hinz, W.A., Virshup, D.M., Ptácek, L.J. and Fu, Y.H. (2001) An hPer2 phosphorylation site mutation in familial advanced sleep phase syndrome. *Science*, **291**, 1040–1043.
3. Xu, Y., Padiath, Q.S., Shapiro, R.E., Jones, C.R., Wu, S.C., Saigoh, N., Saigoh, K., Ptácek, L.J. and Fu, Y.H. (2005) Functional consequences of a CKIdelta mutation causing familial advanced sleep phase syndrome. *Nature*, **434**, 640–644.
4. Ebisawa, T., Uchiyama, M., Kajimura, N., Mishima, K., Kamei, Y., Katoh, M., Watanabe, T., Sekimoto, M., Shibui, K., Kim, K. *et al.* (2001) Association of structural polymorphisms in the human period3 gene with delayed sleep phase syndrome. *EMBO Rep.*, **2**, 342–346.
5. Panda, S., Antoch, M.P., Miller, B.H., Su, A.I., Schook, A.B., Straume, M., Schultz, P.G., Kay, S.A., Takahashi, J.S. and Hogenesch, J.B. (2002) Coordinated transcription of key pathways in the mouse by the circadian clock. *Cell*, **109**, 307–220.
6. Etchegaray, J.P., Lee, C., Wade, P.A. and Reppert, S.M. (2003) Rhythmic histone acetylation underlies transcription in the mammalian circadian clock. *Nature*, **421**, 177–182.
7. Doi, M., Hirayama, J. and Sassone-Corsi, P. (2006) Circadian regulator CLOCK is a histone acetyltransferase. *Cell*, **125**, 497–508.
8. Asher, G., Gatfield, D., Stratmann, M., Reinke, H., Dibner, C., Kreppel, F., Mostoslavsky, R., Alt, F.W. and Schibler, U. (2008) SIRT1 regulates circadian clock gene expression through PER2 deacetylation. *Cell*, **134**, 317–328.
9. Nakahata, Y., Kaluzova, M., Grimaldi, B., Sahar, S., Hirayama, J., Chen, D., Guarente, L.P. and Sassone-Corsi, P. (2008) The NAD^+-dependent deacetylase SIRT1 modulates CLOCK-mediated chromatin remodeling and circadian control. *Cell*, **134**, 329–340.
10. Etchegaray, J.P., Yang, X., DeBruyne, J.P., Peters, A.H., Weaver, D.R., Jenuwein, T. and Reppert, S.M. (2006) The polycomb group protein EZH2 is required for mammalian circadian clock function. *J. Biol. Chem.*, **281**, 21209–21215.
11. Chen, S.T., Choo, K.B., Hou, M.F., Yeh, K.T., Kuo, S.J. and Chang, J.G. (2005) Deregulated expression of the PER1, PER2 and PER3 genes in breast cancers. *Carcinogenesis*, **26**, 1241–1246.
12. Price, J.L., Blau, J., Rothenfluh, A., Abodeely, M., Kloss, B. and Young, M.W. (1998) *double-time* is a novel *Drosophila* clock gene that regulates PERIOD protein accumulation. *Cell*, **94**, 83–95.
13. Shirogane, T., Jin, J., Ang, X.L. and Harper, J.W. (2005) SCFbeta-TRCP controls clock-dependent transcription via casein kinase 1-dependent degradation of the mammalian period-1 (Per1) protein. *J. Biol. Chem.*, **280**, 26863–26872.
14. Busino, L., Bassermann, F., Maiolica, A., Lee, C., Nolan, P.M., Godinho, S.I., Draetta, G.F. and Pagano, M. (2007) SCFFbxl3 controls the oscillation of the circadian clock by directing the degradation of cryptochrome proteins. *Science*, **316**, 900–904.
15. Siepka, S.M., Yoo, S.H., Park, J., Song, W., Kumar, V., Hu, Y., Lee, C. and Takahashi, J.S. (2007) Circadian mutant Overtime reveals F-box protein FBXL3 regulation of cryptochrome and period gene expression. *Cell*, **129**, 1011–1023.
16. Baggs, J.E. and Green, C.B. (2003) Nocturnin, a deadenylase in *Xenopus laevis* retina: a mechanism for posttranscriptional control of circadian-related mRNA. *Curr. Biol.*, **13**, 189–198.
17. Cao, R., Lee, B., Cho, H.Y., Saklayen, S. and Obrietan, K. (2008) Photic regulation of the mTOR signaling pathway in the suprachiasmatic circadian clock. *Mol. Cell. Neurosci.*, **38**, 312–324.
18. Bartel, D.P. (2004) MicroRNAs: genomics, biogenesis, mechanism, and function. *Cell*, **116**, 281–297.
19. Cheng, H.-Y.M., Papp, J.W., Varlamova, O., Dziema, H., Russell, B., Curfman, J.P., Nakazawa, T., Shimizu, K., Okamura, H., Impey, S. and Obrietan, K. (2007) microRNA modulation of circadian-clock period and entrainment. *Neuron*, **54**, 813–829.
20. Yang, M., Lee, J.E., Padgett, R.W. and Edery, I. (2008) Circadian regulation of a limited set of conserved microRNAs in *Drosophila*. *BMC Genomics*, **9**, 83.
21. Gatfield, D., Le Martelot, G., Vejnar, C.E., Gerlach, D., Schaad, O., Fleury-Olela, F., Ruskeepää, A.L., Oresic, M., Esau, C.C., Zdobnov, E.M. and Schibler, U. (2009) Integration of microRNA miR-122 in hepatic circadian gene expression. *Genes Dev.*, **23**, 1313–1326.
22. Kadener, S., Menet, J.S., Sugino, K., Horwich, M.D., Weissbein, U., Nawathean, P., Vagin, V.V., Zamore, P.D., Nelson, S.B. and Rosbash, M. (2009) A role for microRNAs in the *Drosophila* circadian clock. *Genes Dev.*, **23**, 2179–2191.
23. Lim, L.P., Lau, N.C., Garrett-Engele, P., Grimson, A., Schelter, J.M., Castle, J., Bartel, D.P., Linsley, P.S. and Johnson, J.M. (2005) Microarray analysis shows that some microRNAs downregulate large numbers of target mRNAs. *Nature*, **433**, 769–773.
24. Iliopoulos, D., Hirsch, H.A. and Struhl, K. (2009) An epigenetic switch involving NF-kappaB, Lin28, Let-7 MicroRNA, and IL6 links inflammation to cell transformation. *Cell*, **139**, 693–706.
25. Valastyan, S., Reinhardt, F., Benaich, N., Calogrias, D., Szász, A.M., Wang, Z.C., Brock, J.E., Richardson, A.L. and Weinberg, R.A. (2009) A pleiotropically acting microRNA, miR-31, inhibits breast cancer metastasis. *Cell*, **137**, 1032–1046.
26. Xu, N., Papagiannakopoulos, T., Pan, G., Thomson, J.A. and Kosik, K.S. (2009) MicroRNA-145 regulates OCT4, SOX2, and KLF4 and represses pluripotency in human embryonic stem cells. *Cell*, **137**, 647–658.
27. Lewis, B.P., Burge, C.B. and Bartel, D.P. (2005) Conserved seed pairing, often flanked by adenosines, indicates that thousands of human genes are microRNA targets. *Cell*, **120**, 15–20.
28. Zhou, Z., Hong, E.J., Cohen, S., Zhao, W.N., Ho, H.Y., Schmidt, L., Chen, W.G., Lin, Y., Savner, E., Griffith, E.C. *et al.* (2006) Brain-specific phosphorylation of MeCP2 regulates activity-dependent Bdnf transcription, dendritic growth, and spine maturation. *Neuron*, **52**, 255–269.
29. Porterfield, V.M. and Mintz, E.M. (2009) Temporal patterns of light-induced immediate-early gene expression in the suprachiasmatic nucleus. *Neurosci. Lett.*, **463**, 70–73.
30. Chahrour, M., Jung, S.Y., Shaw, C., Zhou, X., Wong, S.T., Qin, J. and Zoghbi, H.Y. (2008) MeCP2, a key contributor to neurological disease, activates and represses transcription. *Science*, **320**, 1224–1229.
31. Ripperger, J.A. and Schibler, U. (2006) Rhythmic CLOCK–BMAL1 binding to multiple E-box motifs drives circadian Dbp transcription and chromatin transitions. *Nat. Genet.*, **38**, 369–374.
32. Mayford, M., Bach, M.E., Huang, Y.Y., Wang, L., Hawkins, R.D. and Kandel, E.R. (1996) Control of memory formation through regulated expression of a CaMKII transgene. *Science*, **274**, 1678–1683.
33. Klose, R.J., Yan, Q., Tothova, Z., Yamane, K., Erdjument-Bromage, H., Tempst, P., Gilliland, D.G., Zhang, Y. and Kaelin, W.G. Jr. (2007) The retinoblastoma binding protein RBP2 is an H3K4 demethylase. *Cell*, **128**, 889–900.
34. Jenuwein, T. and Allis, C.D. (2001) Translating the histone code. *Science*, **293**, 1074–1080.
35. Vo, N. and Goodman, R.H. (2001) CREB-binding protein and p300 in transcriptional regulation. *J. Biol. Chem.*, **276**, 13505–13508.
36. Nan, X., Ng, H.H., Johnson, C.A., Laherty, C.D., Turner, B.M., Eisenman, R.N. and Bird, A. (1998) Transcriptional repression by the methyl-CpG-binding protein MeCP2 involves a histone deacetylase complex. *Nature*, **393**, 386–389.
37. Young, J.I., Hong, E.P., Castle, J.C., Crespo-Barreto, J., Bowman, A.B., Rose, M.F., Kang, D., Richman, R., Johnson, J.M., Berget, S. *et al.* (2005) Regulation of RNA splicing by the methylation-dependent transcriptional repressor methyl-CpG binding protein 2. *Proc. Natl Acad. Sci. USA*, **102**, 17551–17558.
38. Piazza, C.C., Fisher, W., Kiesewetter, K., Bowman, L. and Moser, H. (1990) Aberrant sleep patterns in children with the Rett syndrome. *Brain Dev.*, **12**, 488–493.
39. Mauxion, F., Faux, C. and Séraphin, B. (2008) The BTG2 protein is a general activator of mRNA deadenylation. *EMBO J.*, **27**, 1039–1048.
40. Woo, K.C., Kim, T.D., Lee, K.H., Kim, D.Y., Kim, W., Lee, K.Y. and Kim, K.T. (2009) Mouse period 2 mRNA circadian oscillation is modulated by PTB-mediated rhythmic mRNA degradation. *Nucleic Acids Res.*, **37**, 26–37.
41. Imataka, H., Gradi, A. and Sonenberg, N. (1998) A newly identified N-terminal amino acid sequence of human eIF4G binds poly(A)-binding protein and functions in poly(A)-dependent translation. *EMBO J.*, **17**, 7480–7489.
42. Khaleghpour, K., Svitkin, Y.V., Craig, A.W., DeMaria, C.T., Deo, R.C., Burley, S.K. and Sonenberg, N. (2001) Translational repression by a novel partner of human poly(A) binding protein, Paip2. *Mol. Cell*, **7**, 205–216.
43. Ueda, H.R., Chen, W., Adachi, A., Wakamatsu, H., Hayashi, S., Takasugi, T., Nagano, M., Nakahama, K., Suzuki, Y., Sugano, S. *et al.* (2002) A

transcription factor response element for gene expression during circadian night. *Nature*, **418**, 534–539.
44. Klein, M.E., Lioy, D.T., Ma, L., Impey, S., Mandel, G. and Goodman, R.H. (2007) Homeostatic regulation of MeCP2 expression by a CREB-induced microRNA. *Nat. Neurosci.*, **10**, 1513–1514.
45. Lagos, D., Pollara, G., Henderson, S., Gratrix, F., Fabani, M., Milne, R.S., Gotch, F. and Boshoff, C. (2010) miR-132 regulates antiviral innate immunity through suppression of the p300 transcriptional co-activator. *Nat. Cell Biol.*, **12**, 513–519.
46. Bruce, K., Myers, F.A., Mantouvalou, E., Lefevre, P., Greaves, I., Bonifer, C., Tremethick, D.J., Thorne, A.W. and Crane-Robinson, C. (2005) The replacement histone H2A.Z in a hyperacetylated form is a feature of active genes in the chicken. *Nucleic Acids Res.*, **33**, 5633–5639.
47. Shigeyoshi, Y., Taguchi, K., Yamamoto, S., Takekida, S., Yan, L., Tei, H., Moriya, T., Shibata, S., Loros, J.J., Dunlap, J.C. *et al.* (1997) Light-induced resetting of a mammalian circadian clock is associated with rapid induction of the mPer1 transcript. *Cell*, **91**, 1043–1053.
48. Takumi, T., Matsubara, C., Shigeyoshi, Y., Taguchi, K., Yagita, K., Maebayashi, Y., Sakakida, Y., Okumura, K., Takashima, N. and Okamura, H. (1998) A new mammalian period gene predominantly expressed in the suprachiasmatic nucleus. *Genes Cells*, **3**, 167–176.
49. Yan, L. and Silver, R. (2004) Resetting the brain clock: time course and localization of mPER1 and mPER2 protein expression in suprachiasmatic nuclei during phase shifts. *Eur. J. Neurosci.*, **19**, 1105–1109.
50. Obrietan, K., Impey, S. and Storm, D.R. (1998) Light and circadian rhythmicity regulate MAP kinase activation in the suprachiasmatic nuclei. *Nat. Neurosci.*, **1**, 693–700.
51. Curtis, A.M., Seo, S.B., Westgate, E.J., Rudic, R.D., Smyth, E.M., Chakravarti, D., FitzGerald, G.A. and McNamara, P. (2004) Histone acetyltransferase-dependent chromatin remodeling and the vascular clock. *J. Biol. Chem.*, **279**, 7091–7097.
52. Jones, P.L., Veenstra, G.J., Wade, P.A., Vermaak, D., Kass, S.U., Landsberger, N., Strouboulis, J. and Wolffe, A.P. (1998) Methylated DNA and MeCP2 recruit histone deacetylase to repress transcription. *Nat. Genet.*, **19**, 187–191.
53. Yasui, D.H., Peddada, S., Bieda, M.C., Vallero, R.O., Hogart, A., Nagarajan, R.P., Thatcher, K.N., Farnham, P.J. and Lasalle, J.M. (2007) Integrated epigenomic analyses of neuronal MeCP2 reveal a role for long-range interaction with active genes. *Proc. Natl Acad. Sci. USA*, **104**, 19416–19421.
54. Mnatzakanian, G.N., Lohi, H., Munteanu, I., Alfred, S.E., Yamada, T., MacLeod, P.J., Jones, J.R., Scherer, S.W., Schanen, N.C., Friez, M.J. *et al.* (2004) A previously unidentified MECP2 open reading frame defines a new protein isoform relevant to Rett syndrome. *Nat. Genet.*, **36**, 339–341.
55. Dragich, J.M., Kim, Y.H., Arnold, A.P. and Schanen, N.C. (2007) Differential distribution of the MeCP2 splice variants in the postnatal mouse brain. *J. Comp. Neurol.*, **501**, 526–542.
56. Yamaguchi, S., Mitsui, S., Miyake, S., Yan, L., Onishi, H., Yagita, K., Suzuki, M., Shibata, S., Kobayashi, M. and Okamura, H. (2000) The 5′ upstream region of *mPer1* gene contains two promoters and is responsible for circadian oscillation. *Curr. Biol.*, **10**, 873–876.
57. Yoo, S.H., Ko, C.H., Lowrey, P.L., Buhr, E.D., Song, E.J., Chang, S., Yoo, O.J., Yamazaki, S., Lee, C. and Takahashi, J.S. (2005) A noncanonical E-box enhancer drives mouse Period2 circadian oscillations *in vivo*. *Proc. Natl Acad. Sci. USA*, **102**, 2608–2613.
58. Walton, K.M., Rehfuss, R.P., Chrivia, J.C., Lochner, J.E. and Goodman, R.H. (1992) A dominant repressor of cyclic adenosine 3′,5′-monophosphate (cAMP)-regulated enhancer-binding protein activity inhibits the cAMP-mediated induction of the somatostatin promoter *in vivo*. *Mol. Endocrinol.*, **6**, 647–655.
59. Yanagiya, A., Delbes, G., Svitkin, Y.V., Robaire, B. and Sonenberg, N. (2010) The poly(A)-binding protein partner Paip2a controls translation during late spermiogenesis in mice. *J. Clin. Invest.*, **120**, 3389–3400.
60. Goldstrohm, A.C. and Wickens, M. (2008) Multifunctional deadenylase complexes diversify mRNA control. *Nat. Rev. Mol. Cell. Biol.*, **9**, 337–344.
61. Wormington, M., Searfoss, A.M. and Hurney, C.A. (1996) Overexpression of poly(A) binding protein prevents maturation-specific deadenylation and translational inactivation in *Xenopus oocytes*. *EMBO J.*, **15**, 900–909.
62. Walters, R.W., Bradrick, S.S. and Gromeier, M. (2010) Poly(A)-binding protein modulates mRNA susceptibility to cap-dependent miRNA-mediated repression. *RNA*, **16**, 239–250.
63. Tischkau, S.A., Mitchell, J.W., Tyan, S.H., Buchanan, G.F. and Gillette, M.U. (2003) Ca^{2+}/cAMP response element-binding protein (CREB)-dependent activation of Per1 is required for light-induced signaling in the suprachiasmatic nucleus circadian clock. *J. Biol. Chem.*, **278**, 718–723.
64. Cheng, H.-Y.M., Alvarez-Saavedra, M., Dziema, H., Choi, Y.S., Li, A. and Obrietan, K. (2009) Segregation of expression of *mPeriod* gene homologs in neurons and glia: possible divergent roles of mPeriod1 and mPeriod2 in the brain. *Hum. Mol. Genet.*, **18**, 3110–3124.
65. Cheng, H.-Y.M., Dziema, H., Papp, J., Mathur, D.P., Koletar, M., Ralph, M.R., Penninger, J.M. and Obrietan, K. (2006) The molecular gatekeeper Dexras1 sculpts the photic responsiveness of the mammalian circadian clock. *J. Neurosci.*, **26**, 12984–12995.